CMB seen through random Swiss Cheese

Lavinto, Mikko

2015-10

Lavinto , M & Räsänen , S 2015 , ' CMB seen through random Swiss Cheese ' , Journal of Cosmology and Astroparticle Physics , no. 10 , 057 . https://doi.org/10.1088/1475-7516/2015/10/057

http://hdl.handle.net/10138/310152
https://doi.org/10.1088/1475-7516/2015/10/057

other
acceptedVersion

CMB seen through random Swiss Cheese

Mikko Lavinto and Syksy Räsänen

Physics Department, University of Helsinki and Helsinki Institute of Physics
P.O. Box 64, FIN-00014, University of Helsinki, Finland

E-mail: mikko.lavinto@helsinki.fi, syksy.rasanen@iki.fi

Abstract. We consider a Swiss Cheese model with a random arrangement of Lemaître–Tolman–Bondi holes in ΛCDM cheese. We study two kinds of holes with radius $r_b = 50\ h^{-1}$Mpc, with either an underdense or an overdense centre, called the open and closed case, respectively. We calculate the effect of the holes on the temperature, angular diameter distance and, for the first time in Swiss Cheese models, shear of the CMB. We quantify the systematic shift of the mean and the statistical scatter, and calculate the power spectra.

In the open case, the temperature power spectrum is three orders of magnitude below the linear ISW spectrum. It is sensitive to the details of the hole, in the closed case the amplitude is two orders of magnitude smaller. In contrast, the power spectra of the distance and shear are more robust, and agree with perturbation theory and previous Swiss Cheese results. We do not find a statistically significant mean shift in the sky average of the angular diameter distance, and obtain the 95% limit $|\Delta D_A/\bar{D}_A| \lesssim 10^{-4}$.

We consider the argument that areas of spherical surfaces are nearly unaffected by perturbations, which is often invoked in light propagation calculations. The closed case is consistent with this at 1σ, whereas in the open case the probability is only 1.4%.

Contents

1 Introduction

Inhomogeneities, mean quantities and sampling in light propagation. Studies of the non-linear effect of inhomogeneities on light propagation go back to at least the proposal by Zel'dovich in 1964 that, due to clumping of matter, lines of sight could pass through regions of the universe that are more underdense than the mean, changing the observed distance-redshift relation [1]. The work that followed considered a modification to the optical equations such that light rays see only a constant fraction of the density of a Friedmann–Robertson–Walker (FRW) universe [2–5], now referred to as the Dyer–Roeder formula [6–9]. The applicability of the formalism has since been much studied [10–20], and it has been generalised by making the density sampling factor redshift-dependent and by changing the expansion rate along the light ray [18, 21–29]. The effect of inhomogeneities has been studied also by a variety of other methods; for discussion and references, see e.g. [30].

It is sometimes claimed that even though inhomogeneities can change the distance-redshift relation for some lines of sight, on average it will not deviate from the FRW result. This was argued by Weinberg in 1976 [31], on the basis that because inhomogeneities do not change the number of photons, the total flux through a spherical surface would be conserved. It was already pointed out by Bertotti in 1966 [4] that this argument is wrong, because it assumes that the area of the sphere is unchanged by inhomogeneities, which, however, is precisely the question under study. In general, the area of a sphere can be strongly affected by inhomogeneities, and explicit examples have been presented [32–34], including a case where the metric perturbations around the FRW universe are small [35] (see also [36–40]). The redshift can also change significantly, modifying the distance-redshift relation [41].

It seems that if structures are small compared to the distance travelled by the light and their distribution is statistically homogeneous and isotropic and evolves slowly compared to the time it takes for light to cross them –in short, if light rays sample the structures fairly– then the change in the redshift and distance can be expressed in terms of the average expansion rate [14, 16, 30, 41, 42]. Thus, if the average expansion rate is close to the FRW case, this is expected to be true also for the redshift and the distance. (It is known that if the metric is close to FRW, so are the redshift and the average expansion rate [43].)

Attention has thus focused either on studying the possibility of a large effect of structures on the average expansion rate, i.e. backreaction [44, 45], or analysing the small deviations

in the case when the average expansion rate is close to FRW. A useful treatment of the latter situation is given by Swiss Cheese models, where inhomogeneities are modelled by cutting holes into a spacetime (called the background, or cheese) and replacing them with patches of another spacetime. This was originally done for an Einstein–de Sitter background and Schwarzschild holes [46]. However, the setup can be easily generalised to any FRW background and any Szekeres solution [47], provided the Darmois junction conditions are satisfied [48–51]. If the Szekeres holes are small, long-lived and non-singular (including the absence of surface layers), then the average expansion rate is close to (but not exactly the same as) that of the background [41]. A Swiss Cheese model can be statistically homogeneous and isotropic, if the holes are small and their distribution is chosen appropriately. As Swiss Cheese is an exact solution of the Einstein equation, no perturbative or Newtonian approximations are needed. The model is rather tractable in the sense that the solution to the Einstein equation can be expressed in terms of elliptic integrals, and in the case when cosmological constant is zero, it can be written parametrically in terms of elementary functions [52]. It is also possible to treat more complicated structures than in those exact solutions in which there is no FRW background and the sources are discrete [53–57] (see also [58–68]).

Light propagation in Swiss Cheese models has been extensively studied [13, 17, 18, 20, 69–97]. In particular, Swiss Cheese models have been used to study fluctuations in redshift and distance of the cosmic microwave background (CMB) [81, 98, 99]. Some papers, including recent ones, based either on Swiss Cheese and perturbative calculations, have claimed surprisingly large effects on the distance, given that the average expansion rate has been close to FRW [20, 78, 82, 94, 95, 99, 100]. Such deviations have been due to selection effects, some of which are quite clear and others rather subtle.

We investigate the systematic shift and statistical fluctuations in the redshift, angular diameter distance and shear of the CMB in a Swiss Cheese model. We consider a fully randomized hole distribution in a single fixed spacetime, to avoid biased sampling. This is the first Swiss Cheese CMB calculation of the distance fluctuations with randomised holes in a ΛCDM background. It is also the first study of the CMB shear in a Swiss Cheese model. We use the Lemaître–Tolman–Bondi (LTB) [52, 101–103] solution for the holes, and do the calculation for two different density profiles, one with a central overdensity and another with a central underdensity, for comparison. We calculate the sky maps and power spectra for large scales ($l \lesssim 100$) for the perturbations in redshift, angular diameter distance and integrated null shear generated by the holes between the CMB last scattering surface and the observer. We also study sky averages, including the average of the flux and its inverse. In section 2 we define our model. In section 3 we go through the light propagation calculation. In section 4 we present our results, compare to previous work, with a focus on selection effects and flux conservation arguments, and in section 5 we summarise.

2 Model construction

The Lemaître-Tolman-Bondi solution. The LTB solution [52, 101–103] is the spherically symmetric special case of the Szekeres dust solution. The line element is

$$\mathrm{d}s^2 = -\mathrm{d}t^2 + \frac{R'^2(t,r)}{1+2E(r)}\mathrm{d}r^2 + R^2(t,r)\mathrm{d}\Omega^2 \ , \tag{2.1}$$

where $E(r)$ quantifies the spatial curvature of the shell at coordinate radius r; we denote derivative with respect to r by prime and derivative with respect to t by dot. In units where

$c = G = 1$, the Einstein equation reduces to the equation of motion for R,

$$\dot{R}^2(t,r) = 2E(r) + \frac{2M(r)}{R(t,r)} + \frac{1}{3}\Lambda R^2(t,r) \ , \tag{2.2}$$

where Λ is the cosmological constant and $M(r)$ is a free function related to the dust density as

$$\rho(t,r) = \frac{M'(r)}{4\pi R^2(t,r)R'(t,r)} \ . \tag{2.3}$$

The solution to (2.2) can be found by integrating

$$t - t_B(r) = \int_0^{R(t,r)} \frac{\mathrm{d}R}{\sqrt{\frac{2M}{R} + 2E + \frac{1}{3}\Lambda R^2}} \ , \tag{2.4}$$

and numerically finding the root(s). This integral cannot generally be expressed in terms of elementary functions. We solve it by numerical integration and the algorithm presented in [104, 105]. The bang time function $t_B(r)$ indicates the time of the initial singularity, $R(t_B(r), r) = 0$.

The expansion rate is

$$H(t,r) = \frac{1}{3}\left(\frac{\dot{R}'}{R'} + \frac{2\dot{R}}{R}\right) \ . \tag{2.5}$$

The local homogeneous FRW dust solution is a special case with

$$E = -\frac{1}{2}Kr^2, \qquad M = M_0 r^3, \qquad t_B = 0 \ , \tag{2.6}$$

where K and M_0 are constants, leading to $R(t,r) = a(t)r$.

Junction conditions and shell crossings. Two LTB spacetimes can be joined together into a solution of the Einstein equation without surface layers if and only if the metric and the extrinsic curvature are continuous across the boundary. These are known as the Darmois junction conditions [48, 49]. In order to have a physically viable model, shell crossings also have to be avoided [106]. Since the LTB solution has only dust matter, there are no physical processes that can stop two nearby radial shells from overlapping if they expand at different rates. This leads to a divergence in density and a breakdown of the model. We construct the models so that there are no shell crossings between the time of the big bang and today. Requiring that the LTB holes are free of shell crossings, collapse singularities and surface layers, and that their radius today is much smaller than the Hubble scale, constrains them to have nearly the same volume, average density and total mass as the piece of cheese they displace [41].

Choice of functions. The three free functions $E(r)$, $M(r)$ and $t_B(r)$ specify the model completely. Models with $t_B' \neq 0$ contain decaying modes [107], which would correspond to the universe being far from homogeneous and isotropic at early times. We consider only models where t_B is constant; without loss of generality we then take $t_B = 0$. Given the junction conditions, which fix the value of $M(r)$ on the embedding surface and the assumption that

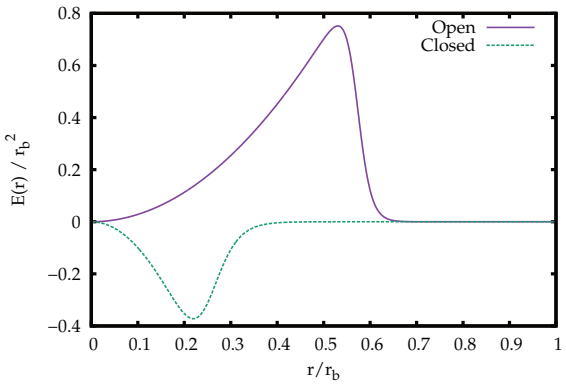

Figure 1. The function $E(r)$ in units of r_b^2.

$M(r)$ is monotonic, its functional form is completely degenerate with the definition of the radial coordinate r. Our choice of $M(r)$ and $E(r)$ is given below, along with $t_B(r)$:

$$M(r) = M_0 r^3 \tag{2.7}$$

$$E(r) = E_0 r^2 \left[1 - \tanh\left(\frac{r - r_t}{r_\sigma}\right)\right] \tag{2.8}$$

$$t_B(r) = 0 \ , \tag{2.9}$$

where M_0 and E_0 are constants. The junction conditions fix $M_0 = \frac{4\pi r_b^3}{3}\bar{\rho}(t_0)$, where bar denotes background quantity and t_0 is the present time. The form of $E(r)$, shown in figure 1, has been chosen because of its smoothness, which makes it possible to speed up the calculation by evaluating R using cubic splines. The constant E_0 determines the sign and magnitude of the spatial curvature in the hole. Parameters r_t and r_σ are the transition radius and width, respectively, where the profile changes smoothly from spatially curved to flat. We choose these constants so that at the embedding boundary $E(r)$ is zero within numerical precision and therefore the Darmois junction conditions are satisfied to good precision, while keeping the model free of shell crossings and also making sure it is very non-linear today; the values are given in table 1. The fact that the Darmois conditions are not exactly satisfied is not a problem. We could make the matching exact by multiplying $E(r)$ with a function that is zero at the boundary and switches rapidly to unity away from it, without affecting the results.

Swiss Cheese. We take the background to be a spatially flat FRW spacetime with dust and a cosmological constant, with present day density parameters $\Omega_\Lambda = 0.7$, $\Omega_m = 0.3$. We consider two kinds of LTB holes, called open and closed, to see how the results depend on the details of the hole. In the open case, there is an underdense void in the centre, surrounded by a thin overdense shell. The closed case has an overdense centre surrounded by an underdensity. The spatial curvature closely follows the density profile, so it is negative at the location of the underdensity and positive at the overdensity. Despite the names, the average spatial curvature over one hole is positive in both cases, although very small, $\langle {}^{(3)}R\rangle_V/(6\bar{H}_0^2) = 5.7 \cdot 10^{-8}$ in the open model and $1.3 \cdot 10^{-8}$ in the closed model, where $\langle\rangle_V$ denotes proper volume average and $\bar{H}_0$ is the background Hubble rate today.

	Open	Closed
r_b	50 h^{-1}Mpc	50 h^{-1}Mpc
r_t/r_b	20/35	5/20
r_σ/r_b	1/35	1/20
E_0	1.41	-5
$\langle\dot{\delta}\rangle_V(t_0)$	$0.156H_0$	$0.010H_0$
$\langle\Delta H/\bar{H}\rangle_V(t_0)$	$-2.0\cdot10^{-7}$	$-1.8\cdot10^{-9}$

Table 1. Parameters of the two models: the embedding radius r_b, transition radius r_t and transition width r_σ and the magnitude of spatial curvature E_0. Also listed are the proper volume averages, denoted by $\langle\rangle_V$, of $\dot{\delta}$ and $\Delta H/\bar{H}$ today.

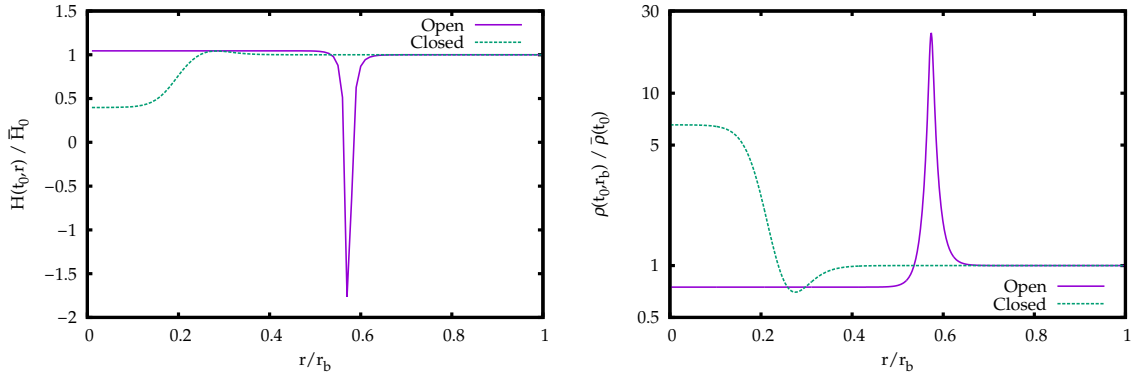

Figure 2. The expansion rate (left) and density (right) of the holes normalised to the background today, as a function of r/r_b. Note that the density plot is logarithmic.

In both cases, the holes are embedded in the background on a comoving boundary with coordinate radius $r_b = 50\ h^{-1}$Mpc. However, the profiles are close to the background already far from the boundary, so the size of the inhomogeneities is smaller than the embedding radius, approximately 30 h^{-1}Mpc for the open model and 20 h^{-1}Mpc for the closed model, as shown in figure 2. In order to avoid shell crossings, there is a trade-off between the non-linearity of the profile and distance of the inhomogeneous features from the boundary, and we have constructed the holes to be clearly in the non-linear regime today.

The energy density in our model does not have a radiation component, so we are missing the early integrated Sachs–Wolfe (ISW) effect. In the real universe, the contribution of radiation to the energy density at the last scattering surface is about 25%. However, we are in any case not interested in modelling the effects at early times, when the holes are in the linear regime. Therefore, we position the sources (as well as the observer) in the cheese. We thus also do not have an ordinary Sachs-Wolfe effect, nor monopole or dipole terms arising from the observer's location (the dipole is generally the dominant contribution; see e.g. [108]). The signal is generated only by secondary effects as the photons propagate through the universe.

We arrange the holes randomly around the observer, with the locations drawn from a uniform distribution and overlapping holes removed. Although this procedure generates some correlation between voids, their distribution is close to uniformly random. The fraction

of the total volume in holes, the packing fraction, is 0.34, close to the packing efficiency of 0.35 in [85, 86]. The effective packing fraction, defined as the fraction of volume in regions that differ significantly from FRW, is smaller, as the profiles tend to the FRW case far from the boundaries, as noted above. We use the same single arrangement of holes for both models and for all geodesics, so correlations due to different rays having passed through the same holes are included. In contrast, most earlier works ([85, 86] being a notable exception) have considered a hole distribution that is dynamically generated along each beam separately or treated statistically [13, 17, 20, 69–72, 74, 77, 81, 91, 92, 97, 99] (see also [109–116]), or have arranged the holes straight on the line of sight [75, 78, 79, 84, 87–89, 99] or in a regular lattice [85, 86, 94, 98].

In the real universe, there are correlated structures of various sizes. It would be possible to construct a model with holes of different radii, profiles and correlated locations to try to match the matter power spectrum. The packing fraction could be increased by using holes of different sizes. By using holes that have a homogeneous region, it is also possible to pack holes inside holes [67]. However, as the holes in Swiss Cheese cannot overlap, merge nor otherwise affect each other gravitationally, its ability to model realistic large scale structure is limited. We restrict ourselves to single size holes with an (almost) uniform distribution.

3 Light propagation

The setup. As long as the wavelength and the wavefront curvature radius are much smaller than spacetime curvature radius, light propagation can be described in the geometrical optics approximation, where light travels as plane waves on null geodesics [117] (p. 93). Let a null geodesic $x^\mu(\lambda)$ be parametrized by an affine parameter λ. Its tangent vector $k^\mu = \frac{\mathrm{d}x^\mu}{\mathrm{d}\lambda}$ satisfies the null condition $k_\mu k^\mu = 0$ and the geodesic equation $k^\mu \nabla_\mu k^\nu = 0$. If the wave vector is given in units where the photon energy at observation is equal to 1, then the redshift measured by an observer with four-velocity u^μ is given by $1 + z = -u_\mu k^\mu$. We consider observers that comove with the dust, so $z = k^t - 1$. The temperature is related to the redshift as $T \propto 1 + z$.

We start the light rays from the observer and follow the evolution of a bundle of null geodesics back in time to the source, using the Sachs formalism to calculate the angular diameter distance and the null shear. We continue the integration until the background redshift reaches 1090, corresponding to the last scattering surface. This choice of direction makes the calculation a lot simpler, and is natural in the sense that all observed geodesics converge at the observer today. However, in reality photons travel from the source towards the observer, so it might seem that this standard procedure solves the wrong physical problem. For the distance, the resolution is well known: backwards integration gives the angular diameter distance D_A, whereas forwards integration gives the luminosity distance D_L divided by $1 + z$ [118]. As the distances are related due to the Etherington reciprocity theorem [118, 119] as $D_L = (1 + z)^2 D_A$, it is simple to correct for this. In appendix A, we prove a similar result for the shear: as long as the integrated null shear is small, it does not depend on whether the initial conditions are set at the observer or the source.

Geodesic equations and redshift. Without loss of generality, we choose the LTB angular coordinates in each hole separately such that the light ray travels on the equator, $\theta = \pi/2$.

Then the null geodesic equations reduce to

$$\frac{\mathrm{d}\theta}{\mathrm{d}\lambda} = 0 \tag{3.1}$$

$$\frac{\mathrm{d}\phi}{\mathrm{d}\lambda} = \frac{c_\phi}{R^2} \tag{3.2}$$

$$\frac{\mathrm{d}z}{\mathrm{d}\lambda} = -\frac{\dot{R}'}{R'}(1+z)^2 + \frac{c_\phi^2}{R^2}\left(\frac{\dot{R}'}{R'} - \frac{\dot{R}}{R}\right) \tag{3.3}$$

$$\frac{\mathrm{d}^2 r}{\mathrm{d}\lambda} = -2\frac{\dot{R}'}{R'}(1+z)\frac{\mathrm{d}r}{\mathrm{d}\lambda} - \left[(1+2E)\frac{R''}{R} - E'\right]\left(\frac{\mathrm{d}r}{\mathrm{d}\lambda}\right)^2 + (1+2E)\frac{c_\phi^2}{R^3 R'} \ , \tag{3.4}$$

where c_ϕ is an integration constant related to the impact parameter. The initial condition for the radial component of the tangent vector can be found using the null condition $k_\mu k^\mu = 0$,

$$\frac{\mathrm{d}r}{\mathrm{d}\lambda} = \frac{1}{R'}\sqrt{(1+z)^2 - \frac{c_\phi^2}{R^2}} \ . \tag{3.5}$$

Distance and null shear. The angular diameter distance from observer O to source S is defined as

$$D_A \equiv \sqrt{\frac{\delta A_S}{\delta \Omega_O}} \ , \tag{3.6}$$

where δA_S is the surface area of the source and $\delta\Omega_O$ is the solid angle in which the source is seen by the observer. We state our results in terms of D_A, which is related to the luminosity distance due to the Etherington reciprocity theorem as

$$D_L = (1+z)^2 D_A \ . \tag{3.7}$$

The evolution of the beam cross section A is given by the Sachs optical equations. The area expansion rate of the beam is

$$\tilde{\theta} \equiv \nabla_\mu k^\mu = \frac{1}{A}\frac{\mathrm{d}A}{\mathrm{d}\lambda} \ , \tag{3.8}$$

and the null shear tensor projected onto a hypersurface orthogonal to the wave vector k^μ with projection tensor $\tilde{h}^\alpha{}_\mu$ is

$$\tilde{\sigma}_{\mu\nu} \equiv \tilde{h}^\alpha{}_\mu \tilde{h}^\beta{}_\nu \nabla_{(\alpha} k_{\beta)} - \frac{1}{2}\theta \tilde{h}_{\mu\nu} \tag{3.9}$$

$$\tilde{\sigma}^2 \equiv \frac{1}{2}\tilde{\sigma}_{\mu\nu}\tilde{\sigma}^{\mu\nu} = (\nabla_\mu k_\nu)(\nabla^\mu k^\nu) - \tilde{\theta}^2 \ . \tag{3.10}$$

The null shear tensor has two real degrees of freedom, and it can be written as

$$\tilde{\sigma}^A{}_B = \begin{pmatrix} \tilde{\sigma}_1 & \tilde{\sigma}_2 \\ \tilde{\sigma}_2 & -\tilde{\sigma}_1 \end{pmatrix} \ , \tag{3.11}$$

where A, B label directions along the lens plane defined by $\tilde{h}_{\alpha\beta}$, and $\tilde{\sigma} = \sqrt{\tilde{\sigma}_1^2 + \tilde{\sigma}_2^2}$.

The Sachs equations are

$$\frac{\mathrm{d}\tilde{\theta}}{\mathrm{d}\lambda}+\frac{1}{2}\tilde{\theta}^2+2\tilde{\sigma}^2=-R_{\mu\nu}k^\mu k^\nu \tag{3.12}$$

$$\tilde{h}^\alpha{}_\mu\tilde{h}^\beta{}_\nu\frac{\mathrm{d}\tilde{\sigma}_{\alpha\beta}}{\mathrm{d}\lambda}+\tilde{\theta}\tilde{\sigma}_{\mu\nu}=-C_{\gamma\alpha\delta\beta}k^\gamma k^\delta\tilde{h}^\alpha{}_\mu\tilde{h}^\beta{}_\nu\ , \tag{3.13}$$

where $R_{\mu\nu}$ is the Ricci tensor and $C_{\gamma\alpha\delta\beta}$ is the Weyl tensor. In terms of the angular diameter distance, (3.12) reads

$$\frac{\mathrm{d}^2D_A}{\mathrm{d}\lambda^2}+\left(\tilde{\sigma}^2+\frac{1}{2}R_{\mu\nu}k^\mu k^\nu\right)D_A=0\ . \tag{3.14}$$

Due to the spherical symmetry of individual LTB solutions, (3.13) and (3.14) can be simplified to

$$\frac{\mathrm{d}^2D_A}{\mathrm{d}\lambda^2}+\left[\tilde{\sigma}^2+4\pi(1+z)^2\rho\right]D_A=0 \tag{3.15}$$

$$\frac{\mathrm{d}\tilde{\sigma}_1}{\mathrm{d}\lambda}+\tilde{\theta}\tilde{\sigma}_1=\frac{c_\phi}{R^2}\left(4\pi\rho-3\frac{M}{R^3}\right)\cos\psi \tag{3.16}$$

$$\frac{\mathrm{d}\tilde{\sigma}_2}{\mathrm{d}\lambda}+\tilde{\theta}\tilde{\sigma}_2=\frac{c_\phi}{R^2}\left(4\pi\rho-3\frac{M}{R^3}\right)\sin\psi\ , \tag{3.17}$$

where ψ is the angle between the line formed by intersection of the lens plane defined by $\tilde{h}_{\alpha\beta}$ with the equator of the first LTB hole, and the line formed by its intersection with the equator of the hole that the beam is going through, so $\psi=0$ for the first hole. The cosmological constant Λ does not enter into the source terms, as it only contributes via terms proportional to $g_{\mu\nu}$, and k^μ is null. We solve these equations backwards in time starting from the observer with the initial conditions

$$D_A|_O=0,\qquad \left.\frac{\mathrm{d}D_A}{\mathrm{d}\lambda}\right|_O=-H_0^{-1},\qquad \tilde{\sigma}_n|_O=0\ . \tag{3.18}$$

Shear has been correctly treated in Swiss Cheese models only rarely [17, 41]. Usually that is not important, because often only the distance is considered, and the effect of the null shear on the distance is generally subdominant to the effect of the density. The shear is also small in our case.

The covariant quantities $\tilde{\theta}$ and $\tilde{\sigma}_n$ can be translated into the perturbative lensing formalism, where the relevant quantity is the amplification matrix [18, 117, 120–122] (see [123] for the second order corrections)

$$\mathcal{A}^A{}_B=\begin{pmatrix}1-\kappa-\gamma_1 & \gamma_2\\ \gamma_2 & 1-\kappa+\gamma_1\end{pmatrix} \tag{3.19}$$

that relates the null geodesic direction at the source to the direction at the observer (see [124] for discussion of the LTB case). The convergence κ corresponds to the change in the bundle area and the integrated null shear γ gives the deformation of the source image. The magnification

$$\mu=\frac{\bar{D}_A^2}{D_A^2}=\det(\mathcal{A})^{-1}=\left[(1-\kappa)^2-\gamma^2\right]^{-1} \tag{3.20}$$

gives the change in the source luminosity relative to the FRW background, with $\gamma \equiv \sqrt{\gamma_1^2 + \gamma_2^2}$.

In the weak lensing limit, $|\kappa| \ll 1$ and $|\gamma_n| \ll 1$, we have

$$\mu = \frac{\bar{D}_A^2}{D_A^2} \simeq 1 + 2\kappa \ , \qquad \gamma_i \simeq \int \mathrm{d}\lambda \tilde{\sigma}_i \ , \tag{3.21}$$

where $\bar{D}_A$ is the angular diameter distance in the background FRW universe, so

$$\frac{\Delta D_A}{\bar{D}_A} \equiv \frac{D_A - \bar{D}_A}{\bar{D}_A} \simeq -\kappa \ . \tag{3.22}$$

Another common way to describe lensing is to use the lensing potential ψ, defined via

$$A_{AB} = \delta_{AB} - \partial_A \partial_B \psi \ , \tag{3.23}$$

for example the Planck lensing results are given in terms of ψ [125]. For more on the relation of the different measures of lensing, see [18, 126].

It is convenient to use the integrated null shear γ instead of $\tilde{\sigma}$, as γ describes the cumulative shearing along the beam path and is independent of the propagation direction (at least for small γ, see appendix A). We give our results in terms of $\Delta T/\bar{T} \equiv (T - \bar{T})/\bar{T}$, $\Delta D_A/\bar{D}_A$ and γ.

4 Results and discussion

Single hole. Let us first consider the effect of a single hole on the temperature, distance and null shear. In the open model, the temperature perturbation is negative in the centre, surrounded by a positive ring, corresponding to the underdense centre and the overdense shell, respectively. For the closed model, the temperature perturbation is everywhere positive. The temperature profiles are shown in figure 3. The maximum amplitude of $\Delta T/\bar{T}$ for a hole at a distance of 200 h^{-1}Mpc is $2 \cdot 10^{-7}$ in the open case and $7 \cdot 10^{-9}$ in the closed case, a ratio of 30. In the open case, the amplitude decreases rapidly with the distance to the hole, as shown in figure 4. For holes close to the observer, the maximum amplotude rises to 10^{-6}. In the closed case, the fall-off is less steep, because the proper volume average of $\dot{\delta}$ over one hole (with $\delta \equiv \rho/\bar{\rho} - 1$) evolves more slowly.

The shell in the open case and the centre in the closed case are in the non-linear regime, as shown in figure 2, so the Rees–Sciama effect [127] is expected to be important in addition to the linear ISW effect. The spherical symmetry leads to stronger cancellation than in ray-tracing through simulated structures [128, 129], where the typical amplitude of the Rees–Sciama effect is $\sim 10^{-6}$, one order of magnitude above our open model and two or three orders of magnitude above our closed model. In the case of a central underdensity, the linear ISW effect and the Rees–Sciama effect enhance each other, whereas for a central overdensity, they pull in opposite directions [129], which may partly explain why the temperature signal in the closed case is smaller than in the open case.

However, the difference in amplitude also reflects the fact that the maximum value of $|E|$ is smaller in the closed model, to avoid shell crossings. To better understand the differences in the two models, let us consider the proper volume averages $\langle\rangle_V$ of $\Delta H/\bar{H} \equiv H/\bar{H} - 1$ and $\dot{\delta} = -3(1+\delta)\Delta H$ over a single hole, given in table 1. Both models expand on average a little slower than the background at present day, $\langle \Delta H/\bar{H} \rangle_V = -2.0 \cdot 10^{-7}$ in the open case and $-1.8 \cdot 10^{-9}$ in the closed case. These numbers are not far from the maximum temperature

amplitudes (though note that $\Delta T/\bar{T}$ can have different sign in the open and closed models). The redshift can be expected to be calculable from the average expansion rate when passing through many structures, but not necessarily in the case of one structure, and it is also important to take the dust shear into account [14, 16, 41, 43], so such a close agreement can be fortuitous, but the order of magnitude is right. In the closed model, the local expansion rate is always positive, whereas in the open model, the volume element in the overdense shell shrinks at late times, as shown in figure 2.

In linear perturbation theory, the temperature perturbation due to the ISW effect is

$$\frac{\Delta T}{\bar{T}} = 2\int \mathrm{d}t\dot{\Phi} \ , \tag{4.1}$$

where the integral is taken along the null geodesic, and the metric perturbation Φ is proportional to δ with a growth function that varies slowly compared to the time it takes to cross a hole. As long as null geodesics sample the spacetime volume fairly, we expect the difference in $\langle\dot{\delta}\rangle_V$ to be indicative of the difference in the temperature perturbation (as noted above, it is a priori not obvious that such an argument applies in the case of a single hole). We have $\langle\dot{\delta}\rangle_V = 0.156H_0$ in the open model and $0.010H_0$ in the closed model, a ratio of 16, in rough agreement with the ratio of temperature anisotropies.

Let us mention that nonlinear voids have been considered as a source of large temperature anisotropies in the CMB [130–135], in particular as a way to explain the so-called Cold Spot. However, no sufficiently large and deep void has been detected, and its existence would be extremely unlikely in the ΛCDM model [108, 129, 136–148]. It has also been argued that the impact of large underdense and overdense regions on the CMB is significantly stronger than predicted in linear theory in the ΛCDM model [149–151], though subsequent studies have found a signal in agreement with such predictions [152–154]. For constraints on exceptional voids from the CMB power spectrum, see [155].

In the open model, the distance perturbation is positive in the centre with a distinct negative spike corresponding to the overdense shell, as shown in figure 5. That is, the image is demagnified in the centre and magnified on the shell. The situation is reversed in the closed model, though the profile is smoother, as in the case of the temperature. The maximum amplitude varies from $\sim 10^{-4}$ to $\sim 10^{-3}$, depending on the distance to the hole. In contrast to temperature perturbations, which are mostly generated by holes close to the observer, perturbations in the angular diameter distance are most strongly produced by holes halfway between source and observer, a common feature in gravitational lensing (see e.g. [117], p. 25). The variation with distance is shown in figure 6 for an open hole; the closed case behaviour is similar. For discussion of lensing by voids, see [93, 156, 157].

The amplitude of the distance perturbation is less sensitive to the choice of profile than the amplitude of the temperature perturbation. The open and closed model results are comparable in amplitude, but have distinct dependence on the viewing angle. There is an argument that the maximum amplitude of the deviation would be of the order $(H_0 r_b)^3$ for the temperature and $(H_0 r_b)^2$ for the distance [72, 158]. Our maximum amplitude of 10^{-6} for the temperature perturbation agrees with this scaling for nearby open holes (for closed holes, the amplitude is smaller). The distance perturbation is indeed $10^{-4} \sim (H_0 r_b)^2$ for holes far from the midpoint between observer and the last scattering surface, but for holes at the optimal distance, it is an order of magnitude larger.

The amplitude of the integrated null shear in both the open and closed cases is $\gamma \sim 10^{-4}$. As with the distance, the angular profile is smoother in the closed case, with the open case

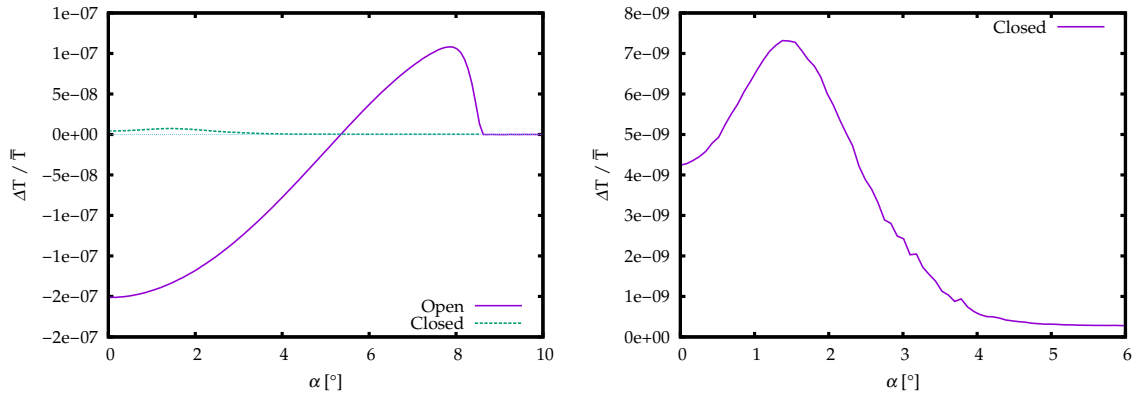

Figure 3. The angular profile of $\Delta T/\bar{T}$ for the open and closed models (left) as a function of the viewing angle α for a single hole, with its centre located at a coordinate distance of 200 h^{-1}Mpc. The result for the closed model is so much smaller that it is also plotted separately (right).

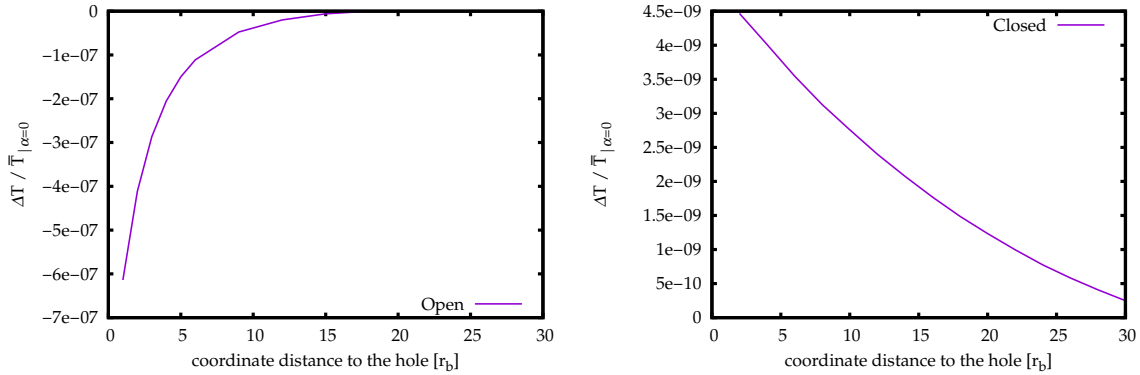

Figure 4. Temperature shift for a radial light ray as a function of the distance to the centre in units of r_b, in the open (left) and closed (right) case.

characterised by a spike corresponding to the light ray passing through the overdense shell, as shown in figure 5.

Multiple holes. As the calculation is too time-intensive to do on very small scales, we focus on multipoles $l \lesssim 100$, corresponding to angles $\gtrsim 1°$. The angular size of a single hole is plotted in figure 6. Therefore we do not have to populate the universe all the way to the last scattering surface, we only need to include holes up to redshift $z \sim 6$, corresponding to an emission time of ~ 1 Gyr and a distance of ~ 6000 h^{-1}Mpc. This is beyond half-way to the last scattering surface (the distance to $z = 1090$ is 9600 h^{-1}Mpc), so we would not expect to find considerably more power on small scales even if we had holes all the way up to $z = 1090$.

We propagate $N = 12\,288$ beams. In table 2 we report the values of $\Delta T/\bar{T}$, $\Delta D_A/\bar{D}_A$ and γ averaged over the sky, with errors calculated using a bootstrap algorithm where random sky maps are generated from the original simulated map. We also give the variation for a single beam for the same quantities. We also give the averages of $(\Delta D_A/\bar{D}_A)^2$, μ and μ^{-1}. If the sky pixels were independent, we would expect the error on the mean to be roughly $1/\sqrt{N}$

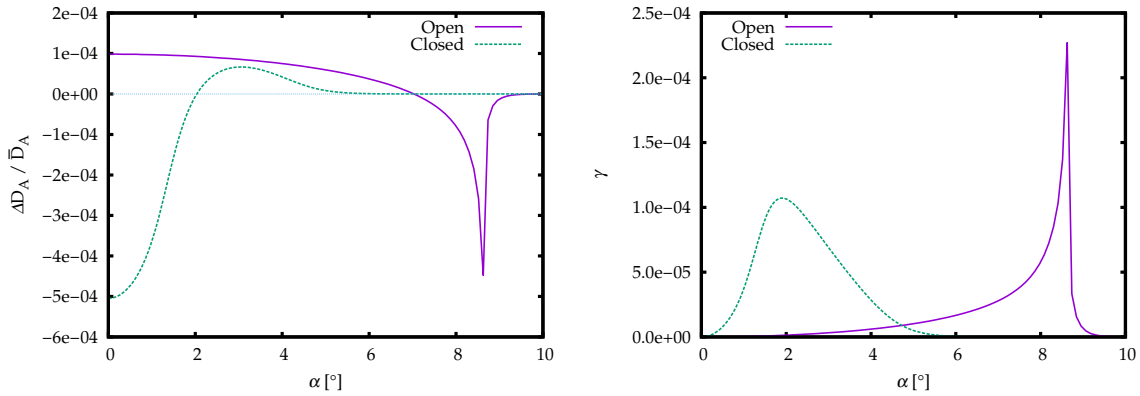

Figure 5. The angular profiles of $\Delta D_A/\bar{D}_A$ (left) and γ (right) for the open and closed models as a function of the viewing angle α for a single hole, with its centre located at a coordinate distance of 200 h^{-1}Mpc.

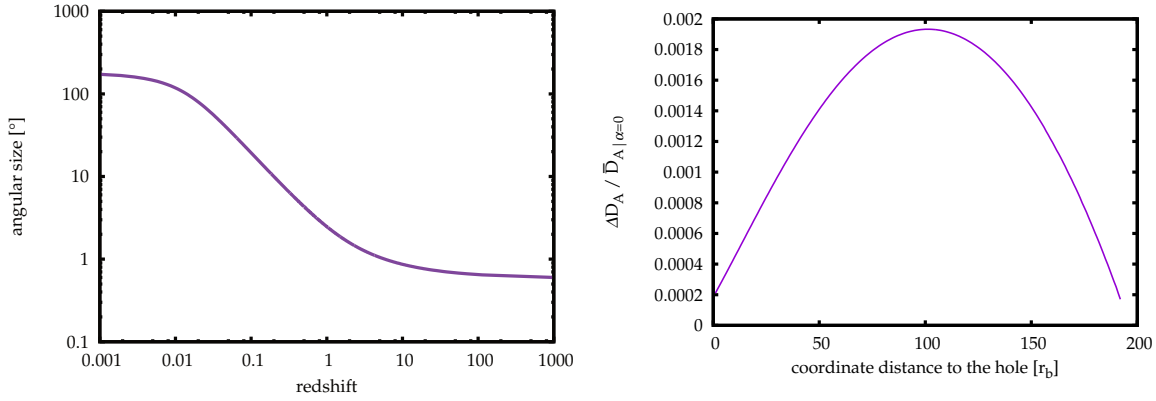

Figure 6. The angular size (left) of a hole ($r_b = 50\ h^{-1}$Mpc) as a function of redshift to the hole centre. The inhomogeneities have radii $\sim 30\ h^{-1}$Mpc and $\sim 20\ h^{-1}$Mpc in the open and closed models, respectively, so they are somewhat smaller. Temperature shift (right) for a radial light ray as a function of the distance to the centre in units of r_b, for the open model.

times the variation for a single beam, and the numbers in table 2 agree quite well with this. The histograms showing the detailed shape of the distribution for single beams are plotted in figure 7, and the bootstrap errors for $\langle \Delta D_A/\bar{D}_A \rangle$ are shown in 8.

The mean temperature shift is $\langle \Delta T/\bar{T} \rangle = (2.15 \pm 0.10) \times 10^{-8}$ in the open case and $(3.17 \pm 0.03) \times 10^{-9}$, an order of magnitude smaller, in the closed case. (Our errors always correspond to one standard deviation.) For the open model, the hot and cold regions cancel to high precision, so the mean value is well below the typical fluctuation range $\sim 10^{-7}$ of a single beam. For the closed model, the temperature perturbation is everywhere positive, so there are no cancellations and the mean is of the same order of magnitude as a typical fluctuation. As the effective packing fraction is small and the temperature signal falls off as a function of distance to the hole, as shown in figure 4, the temperature perturbation along a single line of sight typically gets contributions from only a few holes (more in the closed than in the open case). Therefore the typical fluctuation is much smaller than the maximum fluctuation for a single hole (obtained for a radial light ray), in both cases.

	Open	Closed
$\langle \Delta T/\bar{T} \rangle$	$(2.15 \pm 0.10) \times 10^{-8}$	$(3.17 \pm 0.03) \times 10^{-9}$
$\sigma_{\Delta T/\bar{T}}$	$(9.05 \pm 0.10) \times 10^{-8}$	$(2.13 \pm 0.04) \times 10^{-9}$
$\langle \Delta D_A/\bar{D}_A \rangle$	$(8.5 \pm 4.3) \times 10^{-5}$	$(1.1 \pm 2.4) \times 10^{-5}$
$\langle (\Delta D_A/\bar{D}_A)^2 \rangle$	$(1.65 \pm 0.02) \times 10^{-5}$	$(5.28 \pm 0.08) \times 10^{-6}$
$\sigma_{\Delta D_A/\bar{D}_A}$	$(4.07 \pm 0.03) \times 10^{-3}$	$(2.30 \pm 0.02) \times 10^{-3}$
$\langle \gamma \rangle$	$(1.78 \pm 0.01) \times 10^{-3}$	$(9.85 \pm 0.08) \times 10^{-4}$
σ_γ	$(1.01 \pm 0.02) \times 10^{-3}$	$(6.03 \pm 0.11) \times 10^{-4}$
$\langle \mu \rangle - 1$	$(-1.20 \pm 0.85) \times 10^{-4}$	$(-0.5 \pm 4.7) \times 10^{-5}$
$\langle \mu^{-1} \rangle - 1$	$(1.86 \pm 0.85) \times 10^{-4}$	$(2.7 \pm 4.8) \times 10^{-5}$

Table 2. Mean shift and variation for a single beam for the temperature, distance and shear, as well as the average of the square of the distance deviation, magnification and inverse magnification. Errors are calculated using a bootstrap algorithm, and give one standard deviation. The probability distribution for $\langle \Delta D_A/\bar{D}_A \rangle$ is plotted in figure 8.

The mean shift of the angular diameter distance is $\langle \Delta D_A/\bar{D}_A \rangle = (8.5 \pm 4.3) \cdot 10^{-5}$ in the open model and $(1.1 \pm 2.4) \cdot 10^{-5}$ in the closed model. In contrast to the temperature, the mean shift is not statistically distinguishable from zero, so we can only quote the 95% upper limit $|\langle \Delta D_A/\bar{D}_A \rangle| \lesssim 10^{-4}$, of the same order of magnitude as the signal for a single hole. In both cases, the variation for single beams is at the level 10^{-3}, which explains the large errors. Because of this large variation, it is particularly important to evaluate the errors in the case of the distance, and not just consider the shift in the mean evaluated over a single sky. If the shifts $\langle \Delta D_A/\bar{D}_A \rangle$ were the mean values reported above, we would expect to see them clearly with 3 times more beams in the open case and 50 times more in the closed case.

The mean integrated null shear is $\langle \gamma \rangle \approx 10^{-3}$ in both the open and closed case, of the same order as the typical result for a single ray. The reason is that γ is by definition non-negative, so there can be no cancellations across the sky. The sky average $\langle \gamma \rangle$ is also about an order of magnitude larger than the result for a single hole. The variation for single beams is of the same order of magnitude, so with 12 288 beams, the error on the mean is below 1%.

We calculate power spectra from the CMB maps using the HEALPix [159] package. HEALPix splits the sky into 12 equal sized regions, all of which have N^2 pixels. We used $N = 32$, giving $N_{\text{pix}} = 12\,288$ pixels in total, so we have one beam per pixel. This is enough to calculate the power spectra up to $l < 3N$, though the statistical errors are considerable for $l > 2N$. The resulting sky maps for $\Delta T/\bar{T}$, $\Delta D_A/\bar{D}_A$ and γ are shown in figure 9. As the holes are spherically symmetric, the maps are missing dipolar structures characteristic of the Rees–Sciama effect [129]; it would be possible to model them by using non-spherically symmetric Szekeres holes. Already by eye it is clear that the temperature perturbations are concentrated on large scales, whereas distance and shear have most of their power on small scales. We quantify this by computing the power spectrum for $f(\theta, \phi) = \Delta T/\bar{T}, \Delta D_A/\bar{D}_A, \gamma$

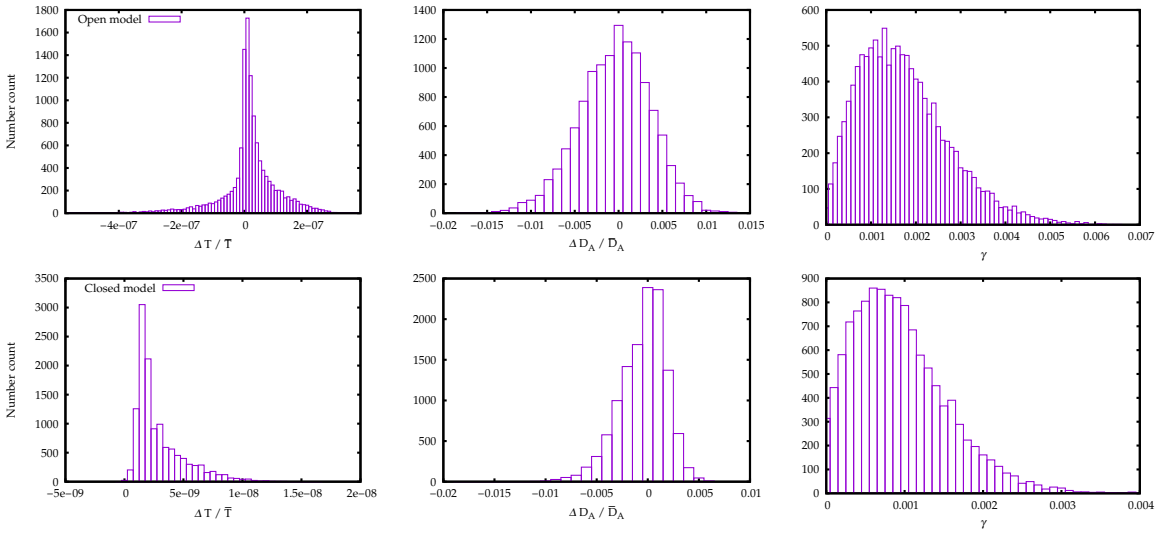

Figure 7. Histograms of $\Delta T/\bar{T}$ (left), $\Delta D_A/\bar{D}_A$ (middle) and γ (right) for open (top) and closed (bottom) models. The mean values and standard deviations are given in table 2.

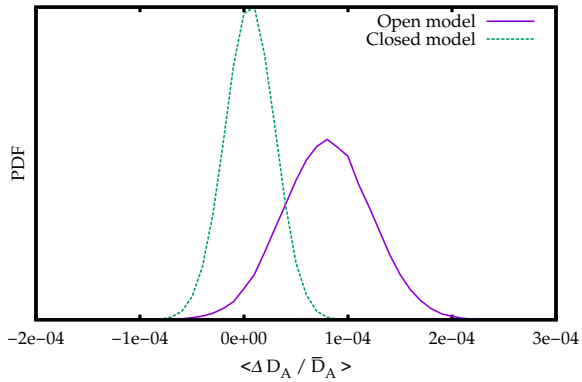

Figure 8. Probability density function for $\langle \Delta D_A/\bar{D}_A \rangle$, estimated using a bootstrap algorithm.

by expanding in terms of the spherical harmonics Y_{lm},

$$C_l^{ff} \equiv \frac{1}{2l+1} \sum_{m=-l}^{l} |a_{lm}^f|^2 \tag{4.2}$$

$$a_{lm}^f \equiv \int_0^{\pi} \mathrm{d}\theta \int_0^{2\pi} \mathrm{d}\phi \; Y_{lm}^*(\theta,\phi) f(\theta,\phi) \; . \tag{4.3}$$

The coefficients a_{lm} are evaluated from the maps by summing over the pixels p,

$$a_{lm} = \frac{4\pi}{N_{\mathrm{pix}}} \sum_{p=0}^{N_{\mathrm{pix}}-1} Y_{lm}^*(\theta_p,\phi_p) f(\theta_p,\phi_p) \; . \tag{4.4}$$

The power spectra of $\Delta T/\bar{T}$, $\Delta D_A/\bar{D}_A$ and γ are plotted in figures 10 and 11, with the full linear perturbation theory CMB spectrum and the linear ISW effect shown for comparison.

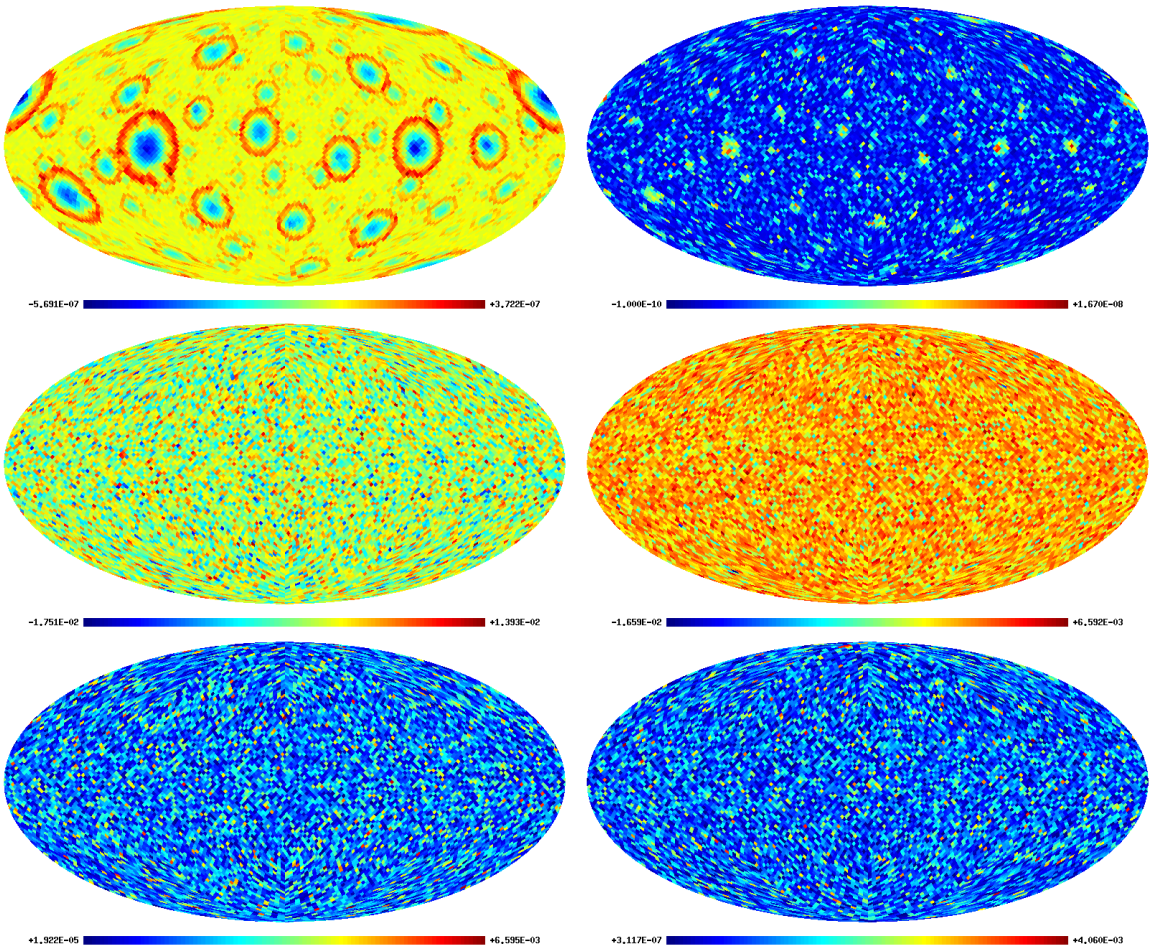

Figure 9. Maps of $\Delta T/\bar{T}$ (top), $\Delta D_A/\bar{D}_A$ (middle) and γ (bottom) for the open (left) and closed (right) model.

The temperature power spectrum for the open model peaks at a multipole between 10 and 20, with an amplitude approximately three orders of magnitude below the linear theory ISW power spectrum, and a bit below the Rees–Sciama effect calculated from perturbation theory and ray-tracing in simulations [127–129]. At $l = 100$ the Swiss Cheese result is two orders of magnitude below the linear ISW effect. The closed model spectrum at its maximum is another three orders of magnitude below the spectrum of the open model. It does not have a peak in the multipole range we consider. This is related to the fact that the temperature profile has less structure, as shown in figure 3. The closed model only produces a faint hot spot, whereas in the open model, the contrasts are stronger, with the cold center surrounded by a hot ring. Also, in the closed case a single ray receives contributions from a larger number of holes at different distances and angular scales, because the temperature perturbation due to the holes goes down more slowly than in the open case, as mentioned above. The small amplitudes of the power spectra, especially on large scales, reflect the fact that the observer and sources are located in the background, and there are almost no correlations between the holes.

The power spectra for the distance and shear are both featureless, with almost constant

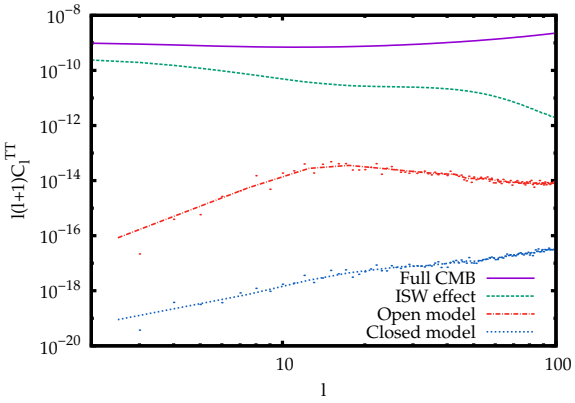

Figure 10. Power spectrum of the temperature anisotropy $\Delta T/\bar{T}$. Plotted are the usual ΛCDM power spectrum, the late-time linear ISW contribution to the ΛCDM result and the power spectra from our Swiss Cheese models. The lines are binned spectra and the dots are individual multipoles.

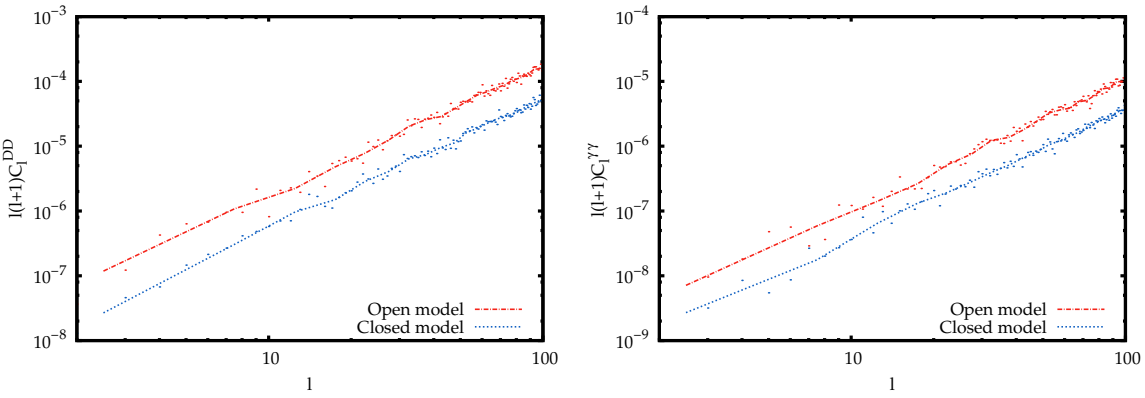

Figure 11. Power spectra for angular diameter distance anisotropy $\Delta D_A/\bar{D}_A$ and shear γ calculated from the Swiss Cheese models. The lines are binned spectra and the dots are individual multipoles.

amplitude of C_l^{DD} and $C_l^{\gamma\gamma}$. The amplitude of the distance power spectrum is $l(l+1)C_l^{DD}(l = 100) = 2 \cdot 10^{-4}$ in the open model, and a factor of 3 smaller in the closed model. For the shear power spectrum, we have $l(l+1)C_l^{\gamma\gamma}(l = 100) = 1 \cdot 10^{-5}$ in the open model and; the closed model result is again down by a factor of 3. These numbers are in agreement with the values of $\sigma_{\Delta D_A/\bar{D}_A}$ and σ_γ listed in table 2.

Comparison with other studies. Let us discuss previous work, some of which has claimed surprisingly large effects on the distance, despite the average expansion rate being close to the FRW case. Such results have come down to selection effects, which were already the focus of the work of Zel'dovich [1]. We can distinguish four different cases of sampling bias.

First, both the distribution of structures and the choice of lines of sight can violate statistical homogeneity and isotropy[1]. In [78, 82, 85, 86, 99], there were large voids perfectly

[1]Models where the observer is at the centre of a void whose radius is of the order of the size of the visible universe are an extreme case [35–40].

aligned so that the light rays pass through their centres, leading to an effect of order unity; a smaller but still sizeable effect on the distance with aligned voids was also found in [84]. Randomisation of the voids strongly reduces the effect [13, 85, 86].

Second, even though the though the distribution of holes may be statistically homogeneous and properly randomised lines of sight may be chosen, the distribution of structures can lack statistical isotropy. In [98] the power spectra of the temperature and the angular diameter distance were calculated in a Swiss Cheese model with a cubic lattice of LTB holes up to $z = 1.92$. The dependence of the signal on the size of the hole was studied, with radii between 3.5 Mpc and 1.75 Gpc considered. The temperature power spectrum due to holes with radius 35 Mpc was found to be of the same order of magnitude as the primary CMB signal. This is unexpectedly large, especially as the model does not have a cosmological constant, so the linear ISW effect vanishes. A possible reason is the higher regularity of the lattice, as suggested in [85, 86]. The fact that $t_B \neq 0$ in [98], and so there is a decaying mode, may also enhance the temperature perturbation. In contrast, the amplitude of the distance power spectrum on small scales is similar to that in our models, with $l(l+1)C_l^{DD}(l = 100) \sim 10^{-4}$, though on large scales the spectrum in [98] is considerably larger than in our case, because it stays flat whereas our amplitude falls. The variation for single beams is comparable to our results, $\sigma_{\Delta D_A/\bar{D}_A} = 4.3 \cdot 10^{-3}$. We conclude that the distance spectrum appears to be less sensitive to model details, and there is more room to change the distance-redshift relation in Swiss Cheese models without having an unacceptably large effect on the CMB than estimated in [98], in agreement with [85, 86].

A third form of bias can arise from not sampling all lines of sight. For example, [20, 94, 95] found the luminosity distance in a Swiss Cheese model to be of the order 10% larger than in the background, using both a hexagonal and a random arrangement of holes with radii from 1 Mpc to 200 Mpc. The large deviation is due to the fact that only light rays that passed sufficiently far from the centres of the Schwarzschild holes were considered, to model opaque clumps of matter. This leads to undersampling the density in the shell around the Schwarzschild hole and a Dyer–Roeder-like distance-redshift relation. The level of bias in point sources such as supernovae due to opaqueness in the real universe is not fully settled [14, 18, 19, 29, 88, 99].

Fourth, even if all lines of sight are considered, such as when studying the CMB (leaving aside sky cuts due to foregrounds), the result can be biased if the lines of sight are not correctly weighted. In [100] it was claimed that there is a systematic increase in the mean angular diameter distance of the order 1% from second order perturbation theory (for calculations of the angular diameter distance in perturbation theory, see [160–172]). However, there was a subtle sampling bias: the average was taken over the ensemble rather than sky directions, an issue that can potentially also arise in other contexts where a statistical treatment of light propagation is used (as opposed to considering one fixed spacetime, as in our case). It was argued in [173] that even though the distance perturbation for a typical light ray is positive, the negative contributions outweigh the positive ones when averaged over the sky. Also, one has to make a careful distinction between perturbations in the flux and in the luminosity distance, as they are not linearly dependent. With these biases taken into account, the effect is reduced by orders of magnitude [173–175] (see also [172]).

These arguments have been related to the assumption of [31] that the area average of the flux (proportional to μ) is conserved if the area of a sphere is unaffected by inhomogeneities. It can be shown that in the same situation the angular average of the inverse flux (proportional to μ^{-1}) is conserved [175, 176]. As discussed in the introduction, this is not true in general.

We can now see how well the conservation holds in our Swiss Cheese universe, whose average properties are by construction close to the FRW case. We have considered angular averages, in which case it follows from $\langle \mu^{-1} \rangle = 1$ straightforwardly, using (3.20) and (3.21), that $\langle \Delta D_A / \bar{D}_A \rangle = -\frac{1}{2} \langle \kappa^2 \rangle = -\frac{1}{2} \langle (\Delta D_A / \bar{D}_A)^2 \rangle$. In particular, this implies that $\langle \Delta D_A / \bar{D}_A \rangle < 0$. As we have noted, we do not have enough beams to see a statistically significant deviation of $\langle \Delta D_A / \bar{D}_A \rangle$ from 0, but we can see whether it is as negative as required by the above relation. The distribution of $\langle \Delta D_A / \bar{D}_A \rangle$ is shown in figure 8, and some numbers are given in table 2. In the closed case, the errors are large, and our results are consistent with the relation $\langle \Delta D_A / \bar{D}_A \rangle = -\frac{1}{2} \langle (\Delta D_A / \bar{D}_A)^2 \rangle$. In the open case, the errors are smaller, and the probability that $\langle \Delta D_A / \bar{D}_A \rangle$ is as small as $-\frac{1}{2} \langle (\Delta D_A / \bar{D}_A)^2 \rangle$ is only 1.4%. Another way of viewing the same thing is to look at $\langle \mu^{-1} \rangle - 1$, given in table 2. In the closed case, zero is within 1σ, whereas in the open case, the probability for zero is 1.4%. We note that, in contrast, $\langle \mu \rangle - 1$ is consistent with zero at the 1σ level in the closed case and 2σ level in the open case, and the corresponding relation $\langle \Delta D_A / \bar{D}_A \rangle = \frac{3}{2} \langle (\Delta D_A / \bar{D}_A)^2 \rangle$ is easily satisfied. The studies [91, 96], discussed below, also find $\langle \Delta D_A / \bar{D}_A \rangle > 0$. Therefore, the assumption that the area of spheres is unperturbed, central to the arguments in [31, 175, 176], does not seem to be a good approximation in these Swiss Cheese models. Using more beams would allow to study the issue in our model with higher statistical significance.

In [162], the power spectrum for the luminosity distance was calculated in linear perturbation theory in a ΛCDM universe (see also [160, 161]). At multipoles $l > 10$ and large redshifts, lensing by structures is the dominant effect. Because of the distance duality relation (3.7), perturbations of the angular diameter and luminosity distance are comparable, $\frac{\Delta D_A}{\bar{D}_A} \simeq \frac{\Delta D_L}{\bar{D}_L}$, as long as the redshift perturbation is much smaller. Their distance power spectrum has a similar shape as in our case, and the amplitude $l(l+1)C_l^{DD}(l = 100) = 3 \cdot 10^{-5}$ is close to our result for the closed model. In our open model the amplitude is an order of magnitude higher.

In [91], a ΛCDM Swiss Cheese model with spherical voids of 35 Mpc radius was studied with $N = 2 \cdot 10^6$ beams up to $z = 2.1$. For $z = 1$, the authors report (translating from the distance modulus to the angular diameter distance) $\langle \Delta D_A / \bar{D}_A \rangle = (1.4 \pm 0.5) \cdot 10^{-3}$. The variation for individual beams is $\sigma_{\Delta D_A / \bar{D}_A} = 0.01$. The shift in the mean is an order of magnitude larger than in our case, and the variation for single beams is a factor of a few larger. One reason may be that in [91] the time spent by the light rays in the cheese is minimised. In [92] halos were included, but the resulting holes are no longer solutions of the Einstein equation, and the treatment is statistical rather than exact. The results were $\langle \Delta D_A / \bar{D}_A \rangle = -(5 \ldots 6) \cdot 10^{-4}$ and $\sigma_{\Delta D_A / \bar{D}_A} = 0.03$, an order of magnitude higher than in our open model. The sign of the mean shift is also the opposite of that in exact in Swiss Cheese calculations.

In [96], a ΛCDM Swiss Cheese model with Szekeres holes that are not spherically symmetric was considered, up to $z = 1.5$. Holes with different radii were studied, including ones with radius 35 Mpc, close to our case, and a density profile somewhat similar to that of our open model. For $z = 1$ the authors report $\langle \Delta D_A / \bar{D}_A \rangle = 4.5 \cdot 10^{-4}$ and $\sigma_{\Delta D_A / \bar{D}_A} = 1.8 \cdot 10^{-3}$ for sources at $z = 1$. They have $N = 1000$, so the error estimate for $\langle \Delta D_A / \bar{D}_A \rangle$ is $0.6 \cdot 10^{-4}$, and the positive mean shift is statistically highly significant. It is somewhat surprising that their standard deviation is smaller than in our model, while the mean distance shift is larger. As noted, we do not find a statistically significant shift in the mean distance, only a limit of $|\langle \Delta D_A / \bar{D}_A \rangle| \lesssim 10^{-4}$. Given that the Szekeres holes in [96] are less symmetric than our spherical holes, we would have expected the deviation for a single beam to be larger [177],

as it takes longer for the inhomogeneities along a light ray to average out.

Observational constraints on fluctuations in the distance to the CMB are mainly from studies of the variation of the multipole location of the acoustic peaks [178, 179], which (for fixed matter content) is a measure of the angular diameter distance [180–182]. The current precision is below the theoretically expected signal.

5 Conclusions

Effect of random holes on the CMB. We have done the first calculation of the redshift, distance and shear of the CMB in a Swiss Cheese model with randomised holes in a ΛCDM background. We have been careful about sampling lines of sight fairly, and have used a spacetime with fixed hole positions drawn from a uniform distribution. We have considered two kinds of LTB holes, with either an over- or underdensity in the centre, called the open and closed model, respectively. The hole radius is $r_b = 50\ h^{-1}$Mpc, but the profile becomes close to the FRW cheese at a radius of about 30 h^{-1}Mpc in the open and 20 h^{-1}Mpc in the closed model.

We find a maximum temperature perturbation for a single hole of $|\Delta T/\bar{T}| \sim 10^{-6} \sim (r_b H_0)^3$ in the open case, for a hole close to the observer; the amplitude falls off sharply with the distance to the hole. The result is sensitive to the hole profile, for the closed case the amplitude is an order of magnitude smaller and the fall-off is less strong. The difference in the order of magnitude corresponds, roughly, to the ratio of the average expansion rate in the open and closed models, and somewhat more closely to the ratio of the proper volume average of the time derivative of the density contrast. The distance perturbation is less sensitive to the details of the hole. For a single hole the distance perturbation has nearly the same amplitude in both models, although the dependence on the viewing angle is distinctive. The maximum amplitude is $\sim 10^{-3}$ for holes located at a distance of $\sim 100 r_b$ from the observer, whereas the typical amplitude is $10^{-4} \sim (r_b H_0)^2$. The amplitude of the integrated null shear is similar, with $\gamma \sim 10^{-4}$ in both the open and closed case.

For the entire distribution of holes, we have calculated the the shift in the mean, variation for a single beam and power spectra for $\Delta T/\bar{T}$, $\Delta D_A/\bar{D}_A$ and γ, using 12 288 beams and an equal number of pixels on the sky. The errors are estimated using a bootstrap algorithm. The sky average of the shift in the temperature is $\langle \Delta T/\bar{T} \rangle = (2.15 \pm 0.10) \times 10^{-8}$ for the open model and $(3.17 \pm 0.03) \times 10^{-9}$ for the closed model, a difference of an order of magnitude, as in the single hole case. For the open model, the power spectrum peaks at a multipole between 10 and 20, but even there it is below the Rees–Sciama effect estimated from perturbation theory and ray-tracing simulations. On all the scales we consider, $l \lesssim 100$, the open model power spectrum is two or more orders of magnitude below the linear theory ISW power spectrum. The closed model power spectrum, in turn, is at least two orders of magnitude below that of the open model.

For the angular diameter distance, we find $\langle \Delta D_A/\bar{D}_A \rangle = (8.5 \pm 4.3) \cdot 10^{-5}$ in the open model and $(1.1 \pm 2.4) \cdot 10^{-5}$ in the closed model. In other words, we do not see a statistically significant systematic shift, we can only quote a 95% limit of $|\langle \Delta D_A/\bar{D}_A \rangle| \lesssim 10^{-4}$. It is important to account for the variation between different sky realisations when drawing conclusions about the mean shift, especially as the typical variation between lines of sight is $\sim 10^{-3}$ for both the open and closed model, much larger than the possible change in the mean. The amplitude of the power spectrum is $l(l+1)C_l^{DD}(l = 100) = 2 \cdot 10^{-4}$ in the open model, and a factor of 3 smaller in the closed model.

For the integrated null shear, we find $\langle\gamma\rangle = (1.78 \pm 0.01) \times 10^{-3}$ in the open model and $(9.85 \pm 0.08) \times 10^{-4}$ in the closed model. Its shift when passing through many holes is larger than the shift for a single hole, unlike for the temperature and distance. The amplitude of the power spectrum is $l(l+1)C_l^{\gamma\gamma}(l = 100) = 1 \cdot 10^{-5}$ for the open model, and the closed model result is again a factor of 3 smaller.

We have compared our results to earlier work, some of which has had selection biases leading to larger results for the distance or temperature. The temperature power spectrum is rather sensitive to the details of the inhomogeneities, with variations of orders of magnitude between different models. The distance power spectrum is more robust and, taking selection effects in account, our results are comparable to most previous Swiss Cheese calculations, as well as results from perturbation theory. However, some works have reported larger mean shifts in the distance, up to $\sim 10^{-3}$.

We have considered the argument that the areas of spheres are unaffected by perturbations, leading to conservation of the angular average of the inverse flux, and the relation $\langle \Delta D_A/\bar{D}_A \rangle = -\frac{1}{2}\langle (\Delta D_A/\bar{D}_A)^2 \rangle$ [31, 175, 176]. Our closed model is consistent with this relation, whereas in the open model the probability that the two sides agree is only 1.4%. Using more beams than our 12 288 would make it possible to draw more definite conclusions.

The CMB null shear has not been calculated using a Swiss Cheese model before. There is much room for refinement, including correlations among the holes, changing the packing fraction and using holes of different sizes and profiles, including non-spherical Szekeres holes. As lensing of the CMB (and large scale structure) is an increasingly important cosmological probe, more realistic Swiss Cheese models could potentially be an interesting way to study it, as they automatically include all relativistic and non-linear effects, without the need for perturbation theory.

Acknowledgments

We thank Pierre Fleury, Austin Peel and Sebastian J. Szybka for correspondence.

A Integrated null shear proof

Let us show that when the null shear $\tilde{\sigma}$ is small, the integrated null shear γ does not depend on whether the initial conditions are set at the observer or at the source. If the null shear is small, we can neglect the term $\tilde{\sigma}^2$ in the distance equation (3.14). In that case (3.14) becomes independent of the shear equation (3.13), which correspondingly becomes linear. The resulting equations can be written as

$$\frac{\mathrm{d}^2 S}{\mathrm{d}\lambda^2} + QS = 0 \tag{A.1}$$

$$\frac{\mathrm{d}\tilde{\sigma}}{\mathrm{d}\lambda} + \tilde{\theta}\tilde{\sigma} = f \ , \tag{A.2}$$

where we have denoted the distance by S, $Q \equiv \frac{1}{2}R_{\mu\nu}k^\mu k^\nu$, $\tilde{\theta} = 2\frac{1}{S}\frac{\mathrm{d}S}{\mathrm{d}\lambda}$ and f is the Weyl tensor source term. There are no indices in (A.2), as $\tilde{\sigma}$ can be considered a complex variable that contains both of the independent degrees of freedom of $\tilde{\sigma}_{\mu\nu}$ (see e.g. [117], p. 106), in which case f is also complex. Equivalently, we could write (A.2) separately for $\tilde{\sigma}_1$ and $\tilde{\sigma}_2$.

We have two different initial conditions for the equations (A.1), (A.2). We can either start from the observer, so that, as in (3.18),

$$S|_O = 0, \qquad \left.\frac{\mathrm{d}S}{\mathrm{d}\lambda}\right|_O = -H_0^{-1}, \qquad \tilde{\sigma}|_O = 0 \ , \tag{A.3}$$

or from the source, in which case we have

$$S|_S = 0, \qquad \left.\frac{\mathrm{d}S}{\mathrm{d}\lambda}\right|_S = A, \qquad \tilde{\sigma}|_S = 0 \ , \tag{A.4}$$

where $A > 0$ is a constant. (Note that setting the initial conditions for S and $\tilde{\sigma}$ at different ends would be inconsistent.) We denote the two cases by the subscripts O and S, so we have four functions, $S_O(\lambda), S_S(\lambda), \tilde{\sigma}_O(\lambda)$ and $\tilde{\sigma}_S(\lambda)$.

From (A.2) we get the solution

$$\tilde{\sigma}_O = S_O(\lambda)^{-2} \int_{\lambda_O}^{\lambda} \mathrm{d}\lambda' S_O(\lambda')^2 f(\lambda') \ , \tag{A.5}$$

and correspondingly for $\tilde{\sigma}_S$ with the substitution $O \to S$. We define

$$\gamma_O \equiv \int_{\lambda_O}^{\lambda_S} \mathrm{d}\lambda \tilde{\sigma}_O(\lambda) = \int_{\lambda_O}^{\lambda_S} \mathrm{d}\lambda S_O(\lambda)^{-2} \int_{\lambda_O}^{\lambda} \mathrm{d}\lambda' S_O(\lambda')^2 f(\lambda') \tag{A.6}$$

$$\gamma_S \equiv \int_{\lambda_S}^{\lambda_O} \mathrm{d}\lambda \tilde{\sigma}_S(\lambda) = \int_{\lambda_S}^{\lambda_O} \mathrm{d}\lambda S_S(\lambda)^{-2} \int_{\lambda_S}^{\lambda} \mathrm{d}\lambda' S_S(\lambda')^2 f(\lambda') \ . \tag{A.7}$$

It is well known that $S_O = D_A$ and that S_S gives $(1+z)D_A$ [118, 119]. Let us now show that the integrated null shear satisfies $\gamma_O = \gamma_S$ (in the case when $\tilde{\sigma}$ small, so that (A.1) applies). As S_O and S_S are solutions of the same differential equation (A.1), they are related as [183][2]

$$S_O(\lambda) = C_O S_S(\lambda) \int_{\lambda_O}^{\lambda} \mathrm{d}\lambda' S_S(\lambda')^{-2} \tag{A.8}$$

$$S_S(\lambda) = C_S S_O(\lambda) \int_{\lambda_S}^{\lambda} \mathrm{d}\lambda' S_O(\lambda')^{-2} \ , \tag{A.9}$$

where $C_O = -S_O(\lambda_S)\frac{\mathrm{d}S_S}{\mathrm{d}\lambda}(\lambda_S)$ and $C_S = -S_S(\lambda_O)\frac{\mathrm{d}S_O}{\mathrm{d}\lambda}(\lambda_O)$. Taking a derivative of either (A.8) or (A.9) shows that $C_O = -C_S$. Partial integration of (A.6) gives

$$\begin{aligned} \gamma_O &= -\int_{\lambda_O}^{\lambda_S} \mathrm{d}\lambda \left[\int_{\lambda_S}^{\lambda} \mathrm{d}\lambda' S_O(\lambda')^{-2}\right] S_O(\lambda)^2 f(\lambda) \\ &= -C_S^{-1} \int_{\lambda_O}^{\lambda_S} \mathrm{d}\lambda S_O(\lambda) S_S(\lambda) f(\lambda) \ , \end{aligned} \tag{A.10}$$

where we have on the second line applied (A.9). Repeating the exercise with γ_S gives the same result, with the change $O \leftrightarrow S$. Given that $C_O = -C_S$ and changing the direction of integration also gives a minus sign, we have the desired equality $\gamma_O = \gamma_S$.

This result also follows from the reciprocity relation for the Jacobi matrix (eq. (35) of [184])[3]. The reciprocity relation is not limited to the case when $\tilde{\sigma}$ is small, but if $\tilde{\sigma}$ is large, its relation of the lensing parameters of the Jacobi matrix is more complicated, and $\gamma_O = \gamma_S$ does not hold, given the definitions (A.6) and (A.7).

[2] We have a different convention for the sign and normalisation of the affine parameter than [183].

[3] We thank Pierre Fleury for pointing this out.

References

[1] Y. B. Zel'dovich, *Observations in a Universe Homogeneous in the Mean*, *Soviet Astronomy* **8** (1964) 13.

[2] V. M. Dashevskii and Y. B. Zel'dovich, *Propagation of Light in a Nonhomogeneous Nonflat Universe II*, *Soviet Astronomy - AJ* **8** (1965) 854.

[3] V. M. Dashevskii and V. I. Slysh, *On the Propagation of Light in a Nonhomogeneous Universe*, *Soviet Astronomy - AJ* **9** (1966) 671.

[4] B. Bertotti, *The Luminosity of Distant Galaxies*, *Royal Society of London Proceedings Series A* **294** (1966) 195–207.

[5] J. E. Gunn, *On the Propagation of Light in Inhomogeneous Cosmologies. I. Mean Effects*, *ApJ* **150** (1967) 737.

[6] C. C. Dyer and R. C. Roeder, *The Distance-Redshift Relation for Universes with no Intergalactic Medium*, *ApJ* **174** (1972) L115.

[7] C. Dyer and R. Roeder, *Distance-Redshift Relations for Universes with Some Intergalactic Medium*, *Astrophys.J.* **180** (1973) L31.

[8] C. C. Dyer and R. C. Roeder, *Observations in Locally Inhomogeneous Cosmological Models*, *ApJ* **189** (1974) 167–176.

[9] R. C. Roeder, *Apparent magnitudes, redshifts, and inhomogeneities in the universe*, *ApJ* **196** (1975) 671–673.

[10] J. Ehlers and P. Schneider, *Self-consistent probabilities for gravitational lensing in inhomogeneous universes*, *A&A* **168** (1986) 57–61.

[11] T. Futamase and M. Sasaki, *Light propagation and the distance-redshift relation in a realistic inhomogeneous universe*, *Phys.Rev.D* **40** (1989) 2502–2510.

[12] M. Kasai, T. Futamase, and F. Takahara, *Angular diameter distance in a clumpy universe*, *Physics Letters A* **147** (1990) 97–105.

[13] R. A. Vanderveld, E. E. Flanagan, and I. Wasserman, *Luminosity distance in 'Swiss cheese' cosmology with randomized voids: I. Single void size*, *Phys.Rev.* **D78** (2008) 083511, [arXiv:0808.1080].

[14] S. Rasanen, *Light propagation in statistically homogeneous and isotropic dust universes*, *JCAP* **0902** (2009) 011, [arXiv:0812.2872].

[15] T. Okamura and T. Futamase, *Distance-Redshift Relation in a Realistic Inhomogeneous Universe*, *Progress of Theoretical Physics* **122** (2009) 511–520, [arXiv:0905.1160].

[16] S. Räsänen, *Light propagation in statistically homogeneous and isotropic universes with general matter content*, *JCAP* **3** (2010) 18, [arXiv:0912.3370].

[17] S. J. Szybka, *On light propagation in Swiss-Cheese cosmologies*, *Phys.Rev.* **D84** (2011) 044011, [arXiv:1012.5239].

[18] C. Clarkson, G. F. Ellis, A. Faltenbacher, R. Maartens, O. Umeh, and J.-P. Uzan, *(Mis-)Interpreting supernovae observations in a lumpy universe*, *Mon.Not.Roy.Astron.Soc.* **426** (2012) 1121–1136, [arXiv:1109.2484].

[19] K. Bolejko and P. G. Ferreira, *Ricci focusing, shearing, and the expansion rate in an almost homogeneous Universe*, *JCAP* **1205** (2012) 003, [arXiv:1204.0909].

[20] P. Fleury, *Swiss-cheese models and the Dyer-Roeder approximation*, *JCAP* **1406** (2014) 054, [arXiv:1402.3123].

[21] E. V. Linder, *Cosmological tests of generalized Friedmann models*, *A&A* **206** (1988) 175–189.

[22] E. V. Linder, *Light propagation in generalized Friedmann universes*, *A&A* **206** (1988) 190–198.

[23] E. V. Linder, *Isotropy of the microwave background by gravitational lensing*, *A&A* **206** (1988) 199–203.

[24] E. V. Linder, *Transition from Clumpy to Smooth Angular Diameter Distances*, *ApJ* **497** (1998) 28–31, [astro-ph/9707349].

[25] E. V. Linder, *Averaging Inhomogeneous Universes: Volume, Angle, Line of Sight*, *ArXiv Astrophysics e-prints* (1998) [astro-ph/9801122].

[26] R. Kantowski, *Lamé equation for the distance redshift in a partially filled beam Friedmann-Lemaître-Robertson-Walker cosmology*, *Phys.Rev.D* **68** (2003), no. 12 123516, [astro-ph/0308419].

[27] T. Mattsson, *Dark energy as a mirage*, *Gen.Rel.Grav.* **42** (2010) 567–599, [arXiv:0711.4264].

[28] K. Bolejko, *Weak lensing and the Dyer-Roeder approximation*, *Mon.Not.Roy.Astron.Soc.* **412** (2011) 1937, [arXiv:1011.3876].

[29] V. Busti, R. Holanda, and C. Clarkson, *Supernovae as probes of cosmic parameters: estimating the bias from under-dense lines of sight*, *JCAP* **1311** (2013) 020, [arXiv:1309.6540].

[30] S. Rasanen, *Evaluating backreaction with the peak model of structure formation*, *JCAP* **0804** (2008) 026, [arXiv:0801.2692].

[31] S. Weinberg, *Apparent luminosities in a locally inhomogeneous universe*, *ApJ* **208** (1976) L1–L3.

[32] N. Mustapha, B. Bassett, C. Hellaby, and G. Ellis, *Shrinking 2. The Distortion of the area distance redshift relation in inhomogeneous isotropic universes*, *Class.Quant.Grav.* **15** (1998) 2363–2379, [gr-qc/9708043].

[33] G. Ellis, B. Bassett, and P. Dunsby, *Lensing and caustic effects on cosmological distances*, *Class.Quant.Grav.* **15** (1998) 2345–2361, [gr-qc/9801092].

[34] G. Ellis and D. M. Solomons, *Caustics of compensated spherical lens models*, *Class.Quant.Grav.* **15** (1998) 2381–2396, [gr-qc/9802005].

[35] K. Enqvist, M. Mattsson, and G. Rigopoulos, *Supernovae data and perturbative deviation from homogeneity*, *JCAP* **9** (2009) 22, [arXiv:0907.4003].

[36] N. Mustapha, C. Hellaby, and G. Ellis, *Large scale inhomogeneity versus source evolution: Can we distinguish them observationally?*, *Mon.Not.Roy.Astron.Soc.* **292** (1997) 817–830, [gr-qc/9808079].

[37] K. Enqvist, *Lemaitre-Tolman-Bondi model and accelerating expansion*, *Gen.Rel.Grav.* **40** (2008) 451–466, [arXiv:0709.2044].

[38] J. Garcia-Bellido and T. Haugbølle, *Looking the void in the eyes - the kSZ effect in LTB models*, *JCAP* **0809** (2008) 016, [arXiv:0807.1326].

[39] K. Bolejko, M.-N. Célérier, and A. Krasiński, *Inhomogeneous cosmological models: exact solutions and their applications*, *Classical and Quantum Gravity* **28** (2011), no. 16 164002, [arXiv:1102.1449].

[40] P. Sundell, E. Mörtsell, and I. Vilja, *Can a void mimic the* Λ *in* Λ*CDM?*, arXiv:1503.08045.

[41] M. Lavinto, S. Räsänen, and S. J. Szybka, *Average expansion rate and light propagation in a cosmological Tardis spacetime*, *JCAP* **1312** (2013) 051, [arXiv:1308.6731].

[42] P. Bull and T. Clifton, *Local and nonlocal measures of acceleration in cosmology*, *Phys.Rev.D* **85** (2012), no. 10 103512, [arXiv:1203.4479].

[43] S. Rasanen, *Light propagation and the average expansion rate in near-FRW universes*, *Phys.Rev.* **D85** (2012) 083528, [arXiv:1107.1176].

[44] T. Buchert and S. Räsänen, *Backreaction in late-time cosmology*, *Ann.Rev.Nucl.Part.Sci.* **62** (2012) 57–79, [arXiv:1112.5335].

[45] S. Räsänen, *Backreaction: directions of progress*, *Class.Quant.Grav.* **28** (2011) 164008, [arXiv:1102.0408].

[46] A. Einstein and E. G. Straus, *The influence of the expansion of space on the gravitation fields surrounding the individual stars*, *Rev.Mod.Phys.* **17** (1945) 120–124.

[47] P. Szekeres, *A Class of Inhomogeneous Cosmological Models*, *Commun.Math.Phys.* **41** (1975) 55.

[48] G. Darmois, *Les équations de la gravitation einsteinienne*. Gauthier-Villars, 1927.

[49] W. Israel, *Singular hypersurfaces and thin shells in general relativity*, *Nuovo Cim.* **B44S10** (1966) 1. Erratum in *Nuovo Cim.* **B48** (1967) 463.

[50] W. B. Bonnor and P. A. Vickers, *Junction conditions in general relativity*, *General Relativity and Gravitation* **13** (1981) 29–36.

[51] M. Carrera and D. Giulini, *On the influence of global cosmological expansion on the dynamics and kinematics of local systems*, arXiv:0810.2712.

[52] J. Plebanski and A. Krasinski, *An introduction to general relativity and cosmology*. Cambridge University Press, 2006.

[53] T. Clifton and P. G. Ferreira, *Archipelagian cosmology: Dynamics and observables in a universe with discretized matter content*, *Phys.Rev.D* **80** (2009), no. 10 103503, [arXiv:0907.4109].

[54] T. Clifton and P. G. Ferreira, *Errors in estimating Ω_{Lambda} due to the fluid approximation*, *JCAP* **10** (2009) 26, [arXiv:0908.4488].

[55] T. Clifton, P. G. Ferreira, and K. O'Donnell, *Improved treatment of optics in the Lindquist-Wheeler models*, *Phys.Rev.D* **85** (2012), no. 2 023502, [arXiv:1110.3191].

[56] R. G. Liu, *The Lindquist-Wheeler formulation of lattice universes*, arXiv:1501.05169.

[57] V. A. Sanghai and T. Clifton, *Post-Newtonian Cosmological Modelling*, *Phys.Rev.* **D91** (2015) 103532, [arXiv:1503.08747].

[58] T. Clifton, K. Rosquist, and R. Tavakol, *An Exact quantification of backreaction in relativistic cosmology*, *Phys.Rev.* **D86** (2012) 043506, [arXiv:1203.6478].

[59] C.-M. Yoo, H. Abe, K.-i. Nakao, and Y. Takamori, *Black Hole Universe: Construction and Analysis of Initial Data*, *Phys.Rev.* **D86** (2012) 044027, [arXiv:1204.2411].

[60] J.-P. Bruneton and J. Larena, *Dynamics of a lattice Universe: The dust approximation in cosmology*, *Class.Quant.Grav.* **29** (2012) 155001, [arXiv:1204.3433].

[61] E. Bentivegna and M. Korzynski, *Evolution of a periodic eight-black-hole lattice in numerical relativity*, *Class.Quant.Grav.* **29** (2012) 165007, [arXiv:1204.3568].

[62] J.-P. Bruneton and J. Larena, *Observables in a lattice Universe*, *Class.Quant.Grav.* **30** (2013) 025002, [arXiv:1208.1411].

[63] J. Larena, *The fitting problem in a lattice Universe*, *Springer Proc.Phys.* **157** (2014) 385–392, [arXiv:1210.2161].

[64] J.-P. Bruneton, *A lattice Universe as a toy-model for inhomogeneous cosmology*, arXiv:1303.0174.

[65] E. Bentivegna, *Black-hole lattices*, *Springer Proc.Math.Stat.* **60** (2014) 143–146, [arXiv:1307.7673].

[66] M. Korzyński, *Backreaction and continuum limit in a closed universe filled with black holes*, *Class.Quant.Grav.* **31** (2014) 085002, [arXiv:1312.0494].

[67] M. Korzyński, *Nonlinear effects of general relativity from multiscale structure*, arXiv:1412.3865.

[68] M. Korzyński, I. Hinder, and E. Bentivegna, *On the vacuum Einstein equations along curves with a discrete local rotational and reflection symmetry*, arXiv:1505.05760.

[69] R. Kantowski, *Corrections in the Luminosity-Redshift Relations of the Homogeneous Fried-Mann Models*, *ApJ* **155** (1969) 89.

[70] R. Kantowski, T. Vaughan, and D. Branch, *The Effects of Inhomogeneities on Evaluating the Deceleration Parameter Q 0*, *ApJ* **447** (1995) 35, [astro-ph/9511108].

[71] R. Kantowski, *The Effects of Inhomogeneities on Evaluating the Mass Parameter Ω_m and the Cosmological Constant Λ*, *ApJ* **507** (1998) 483–496, [astro-ph/9802208].

[72] N. Sugiura, K.-i. Nakao, D. Ida, N. Sakai, and H. Ishihara, *How do nonlinear voids affect light propagation?*, *Prog.Theor.Phys.* **103** (2000) 73–89, [astro-ph/9912414].

[73] C.-M. Claudel, *Cumulative gravitational lensing in Newtonian perturbations of Friedman-Robertson-Walker cosmologies*, *Proc.Roy.Soc.Lond.* **A456** (2000) 1455–1482, [gr-qc/0005097].

[74] R. Kantowski and R. C. Thomas, *Distance-Redshift in Inhomogeneous Ω_0=1 Friedmann-Lemaître-Robertson-Walker Cosmology*, *ApJ* **561** (2001) 491–495, [astro-ph/0011176].

[75] N. Brouzakis, N. Tetradis, and E. Tzavara, *The Effect of Large-Scale Inhomogeneities on the Luminosity Distance*, *JCAP* **0702** (2007) 013, [astro-ph/0612179].

[76] T. Biswas and A. Notari, *Swiss-Cheese Inhomogeneous Cosmology and the Dark Energy Problem*, *JCAP* **0806** (2008) 021, [astro-ph/0702555].

[77] N. Brouzakis, N. Tetradis, and E. Tzavara, *Light Propagation and Large-Scale Inhomogeneities*, *JCAP* **0804** (2008) 008, [astro-ph/0703586].

[78] V. Marra, E. W. Kolb, S. Matarrese, and A. Riotto, *On cosmological observables in a swiss-cheese universe*, *Phys.Rev.* **D76** (2007) 123004, [arXiv:0708.3622].

[79] V. Marra, E. W. Kolb, and S. Matarrese, *Light-cone averages in a swiss-cheese Universe*, *Phys.Rev.* **D77** (2008) 023003, [arXiv:0710.5505].

[80] K. Bolejko, *Light propagation through large-scale inhomogeneities in the Universe and its impact on cosmological observations*, *EAS Publ.Ser.* **30** (2008) 349–352, [arXiv:0804.1826].

[81] K. Bolejko, *The Szekeres Swiss Cheese model and the CMB observations*, *Gen.Rel.Grav.* **41** (2009) 1737–1755, [arXiv:0804.1846].

[82] V. Marra, *On cosmological observables in a swiss-cheese universe*, arXiv:0805.4233.

[83] S. Ghassemi, S. Khoeini-Moghaddam, and R. Mansouri, *Lensing effects in inhomogeneous cosmological models*, *Phys.Rev.D* **79** (2009), no. 10 102002, [arXiv:0901.0340].

[84] T. Clifton and J. Zuntz, *Hubble diagram dispersion from large-scale structure*, *MNRAS* **400** (2009) 2185–2199, [arXiv:0902.0726].

[85] V. Kostov, *Average luminosity distance in inhomogeneous universes*, *JCAP* **1004** (2010) 001, [arXiv:0910.2611].

[86] V. A. Kostov, *Average luminosity distance in inhomogeneous universes*. PhD thesis, The University of Chicago, 2010.

[87] K. Bolejko and M.-N. Celerier, *Szekeres Swiss-Cheese model and supernova observations*, *Phys.Rev.* **D82** (2010) 103510, [arXiv:1005.2584].

[88] K. Bolejko, *Conceptual problems in detecting the evolution of dark energy when using distance measurements*, *A&A* **525** (2011) A49, [arXiv:1006.3348].

[89] V. Marra and A. Notari, *Observational constraints on inhomogeneous cosmological models without dark energy*, *Classical and Quantum Gravity* **28** (2011), no. 16 164004, [arXiv:1102.1015].

[90] A. de Lavallaz and M. Fairbairn, *Effects of voids on the reconstruction of the equation of state of Dark Energy*, *Phys.Rev.* **D84** (2011) 083005, [arXiv:1106.1611].

[91] E. E. Flanagan, N. Kumar, I. Wasserman, and R. A. Vanderveld, *Luminosity distance in Swiss cheese cosmology with randomized voids. II. Magnification probability distributions*, *Phys.Rev.* **D85** (2012) 023510, [arXiv:1109.1873].

[92] E. E. Flanagan, N. Kumar, and I. Wasserman, *Luminosity distance in Swiss cheese cosmology with randomized voids and galaxy halos*, *Phys.Rev.* **D88** (2013), no. 4 043004, [arXiv:1207.3711].

[93] K. Bolejko, C. Clarkson, R. Maartens, D. Bacon, N. Meures, and E. Beynon, *Antilensing: The Bright Side of Voids*, *Physical Review Letters* **110** (2013), no. 2 021302, [arXiv:1209.3142].

[94] P. Fleury, H. Dupuy, and J.-P. Uzan, *Interpretation of the Hubble diagram in a nonhomogeneous universe*, *Phys.Rev.* **D87** (2013), no. 12 123526, [arXiv:1302.5308].

[95] P. Fleury, H. Dupuy, and J.-P. Uzan, *Can all cosmological observations be accurately interpreted with a unique geometry?*, *Phys.Rev.Lett.* **111** (2013) 091302, [arXiv:1304.7791].

[96] A. Peel, M. A. Troxel, and M. Ishak, *Effect of inhomogeneities on high precision measurements of cosmological distances*, *Phys. Rev.* **D90** (2014), no. 12 123536, [arXiv:1408.4390]. [Erratum: Phys. Rev.D92,no.2,029901(2015)].

[97] S. Koksbang and S. Hannestad, *Studying the precision of ray tracing techniques with Szekeres models*, arXiv:1506.09127.

[98] W. Valkenburg, *Swiss Cheese and a Cheesy CMB*, *JCAP* **0906** (2009) 010, [arXiv:0902.4698].

[99] K. Bolejko, *The effect of inhomogeneities on the distance to the last scattering surface and the accuracy of the CMB analysis*, *JCAP* **1102** (2011) 025, [arXiv:1101.3338].

[100] C. Clarkson, O. Umeh, R. Maartens, and R. Durrer, *What is the distance to the CMB?*, arXiv:1405.7860.

[101] G. Lemaitre, *A homogeneous Universe of constant mass and growing radius accounting for the radial velocity of extragalactic nebulae*, *Annales Soc.Sci.Brux.Ser.I Sci.Math.Astron.Phys.* **A47** (1927) 49–59.

[102] R. C. Tolman, *Effect of imhomogeneity on cosmological models*, *Proc.Nat.Acad.Sci.* **20** (1934) 169–176.

[103] H. Bondi, *Spherically symmetrical models in general relativity*, *Mon.Not.Roy.Astron.Soc.* **107** (1947) 410–425.

[104] B. Carlson, *Numerical computation of real or complex elliptic integrals*, *Numerical Algorithms* **10** (1995) 13–26, [math/9409227].

[105] W. Valkenburg, *Complete solutions to the metric of spherically collapsing dust in an expanding spacetime with a cosmological constant*, *General Relativity and Gravitation* **44** (2012) 2449–2476, [arXiv:1104.1082].

[106] C. Hellaby and K. Lake, *Shell crossings and the Tolman model*, *Astrophys.J.* **290** (1985) 381. Erratum in ApJ300 (1986) 461.

[107] J. Silk, *Large-scale inhomogeneity of the Universe - Spherically symmetric models*, *A&A* **59** (1977) 53–58.

[108] S. Nadathur, M. Lavinto, S. Hotchkiss, and S. Räsänen, *Can a supervoid explain the Cold Spot?*, *Phys.Rev.* **D90** (2014), no. 10 103510, [arXiv:1408.4720].

[109] D. E. Holz and R. M. Wald, *A New method for determining cumulative gravitational lensing effects in inhomogeneous universes*, *Phys.Rev.* **D58** (1998) 063501, [astro-ph/9708036].

[110] D. E. Holz, *Lensing and high-z supernova surveys*, *Astrophys.J.* **506** (1998) L1, [astro-ph/9806124].

[111] K. Kainulainen and V. Marra, *Supernovae observations in a "meatball" universe with a local void*, *Phys.Rev.D* **80** (2009), no. 12 127301, [arXiv:0906.3871].

[112] K. Kainulainen and V. Marra, *New stochastic approach to cumulative weak lensing*, *Phys.Rev.D* **80** (2009), no. 12 123020, [arXiv:0909.0822].

[113] K. Kainulainen and V. Marra, *Impact of cosmic inhomogeneities on SNe observations*, in *American Institute of Physics Conference Series* (J.-M. Alimi and A. Fuözfa, eds.), vol. 1241 of *American Institute of Physics Conference Series*, pp. 1043–1050, 2010. arXiv:0911.5584.

[114] L. Amendola, K. Kainulainen, V. Marra, and M. Quartin, *Large-Scale Inhomogeneities May Improve the Cosmic Concordance of Supernovae*, *Physical Review Letters* **105** (2010), no. 12 121302, [arXiv:1002.1232].

[115] K. Kainulainen and V. Marra, *Accurate modeling of weak lensing with the stochastic gravitational lensing method*, *Phys.Rev.D* **83** (2011), no. 2 023009, [arXiv:1011.0732].

[116] K. Kainulainen and V. Marra, *Weak lensing observables in the halo model*, *Phys.Rev.D* **84** (2011), no. 6 063004, [arXiv:1101.4143].

[117] E. F. P. Schneider, J. Ehlers, *Gravitational Lenses*. Springer, 1992.

[118] G. Ellis, *Relativistic cosmology*, *Gen.Rel.Grav.* **41** (2009) 581–660.

[119] I. M. H. Etherington, *On the Definition of Distance in General Relativity.*, *Philosophical Magazine* **15** (1933) 761.

[120] M. Bartelmann and P. Schneider, *Weak gravitational lensing*, *Phys.Rept.* **340** (2001) 291–472, [astro-ph/9912508].

[121] A. Lewis and A. Challinor, *Weak gravitational lensing of the cmb*, *Phys. Rept.* **429** (2006) 1–65, [astro-ph/0601594].

[122] D. Hanson, A. Challinor, and A. Lewis, *Weak lensing of the CMB*, *General Relativity and Gravitation* **42** (Sept., 2010) 2197–2218, [arXiv:0911.0612].

[123] C. Clarkson, *The general theory of secondary weak gravitational lensing*, arXiv:1503.08660.

[124] G. Fanizza and F. Nugier, *Lensing in the geodesic light-cone coordinates and its (exact) illustration to an off-center observer in Lemaitre-Tolman-Bondi models*, *JCAP* **1502** (2015), no. 02 002, [arXiv:1408.1604].

[125] **Planck** Collaboration, P. Ade et al., *Planck 2015 results. XV. Gravitational lensing*, arXiv:1502.01591.

[126] P. Schneider, T. Eifler, and E. Krause, *COSEBIs: Extracting the full E-/B-mode information from cosmic shear correlation functions*, *A&A* **520** (2010) A116, [arXiv:1002.2136].

[127] M. Rees and D. Sciama, *Large scale Density Inhomogeneities in the Universe*, *Nature* **217** (1968) 511–516.

[128] U. Seljak, *Rees-Sciama effect in a CDM universe*, *Astrophys.J.* **460** (1996) 549, [astro-ph/9506048].

[129] Y.-C. Cai, S. Cole, A. Jenkins, and C. S. Frenk, *Full-sky map of the ISW and Rees-Sciama effect from Gpc simulations*, *MNRAS* **407** (2010) 201–224, [arXiv:1003.0974].

[130] E. Martinez-Gonzalez, J. L. Sanz, and J. Silk, *Anisotropies in the microwave sky due to nonlinear structures*, *ApJ* **355** (1990) L5–L9.

[131] E. Martinez-Gonzalez and J. L. Sanz, *CMB Anisotropies Generated by Cosmic Voids and Great Attractors*, *MNRAS* **247** (1990) 473–478.

[132] M. Panek, *Cosmic background radiation anisotropies from cosmic structures - Models based on the Tolman solution*, *ApJ* **388** (1992) 225–233.

[133] J. V. Arnau, M. J. Fullana, L. Monreal, and D. Saez, *On the microwave background anisotropies produced by nonlinear voids*, *ApJ* **402** (Jan., 1993) 359–368.

[134] M. J. Fullana, J. V. Arnau, and D. Saez, *On the microwave background anisotropy produced by big voids in open universes*, *MNRAS* **280** (1996) 1181–1189, [astro-ph/9601154].

[135] K. Tomita and K. T. Inoue, *Second order gravitational effects on CMB temperature anisotropy in Λ dominated flat universes*, *Phys.Rev.D* **77** (2008), no. 10 103522, [arXiv:0712.1291].

[136] K. T. Inoue and J. Silk, *Local Voids as the Origin of Large-Angle Cosmic Microwave Background Anomalies. I.*, *ApJ* **648** (2006) 23–30, [astro-ph/0602478].

[137] L. Rudnick, S. Brown, and L. R. Williams, *Extragalactic Radio Sources and the WMAP Cold Spot*, *ApJ* **671** (Dec., 2007) 40–44, [arXiv:0704.0908]. Erratum in ApJ**678** (2008) 1531.

[138] M. Cruz, E. Martínez-González, P. Vielva, J. M. Diego, M. Hobson, and N. Turok, *The CMB cold spot: texture, cluster or void?*, *MNRAS* **390** (2008) 913–919, [arXiv:0804.2904].

[139] N. Sakai and K. T. Inoue, *Cosmic Microwave Background Anisotropy from Nonlinear Structures in Accelerating Universes*, *Phys. Rev.* **D78** (2008) 063510, [arXiv:0805.3446].

[140] I. Masina and A. Notari, *The cold spot as a large void: Rees-Sciama effect on CMB power spectrum and bispectrum*, *JCAP* **2** (Feb., 2009) 19, [arXiv:0808.1811].

[141] K. M. Smith and D. Huterer, *No evidence for the cold spot in the NVSS radio survey*, *Mon. Not. Roy. Astron. Soc.* **403** (2010) 2, [arXiv:0805.2751].

[142] I. Masina and A. Notari, *The cold spot as a large void: lensing effect on CMB two and three point correlation functions*, *JCAP* **7** (July, 2009) 35, [arXiv:0905.1073].

[143] B. R. Granett, I. Szapudi, and M. C. Neyrinck, *Galaxy Counts on the Cosmic Microwave Background Cold Spot*, *ApJ* **714** (May, 2010) 825–833, [arXiv:0911.2223].

[144] M. N. Bremer, J. Silk, L. J. M. Davies, and M. D. Lehnert, *A redshift survey towards the cosmic microwave background cold spot*, *MNRAS* **404** (May, 2010) L69–L73, [arXiv:1004.1178].

[145] K. T. Inoue, N. Sakai, and K. Tomita, *Evidence of Quasi-linear Super-structures in the Cosmic Microwave Background and Galaxy Distribution*, *ApJ* **724** (Nov., 2010) 12–25, [arXiv:1005.4250].

[146] K. T. Inoue, *On the origin of the cold spot*, *MNRAS* **421** (2012) 2731–2736, [arXiv:1109.4527].

[147] I. Szapudi et al., *Detection of a Supervoid Aligned with the Cold Spot of the Cosmic Microwave Background*, *Mon. Not. Roy. Astron. Soc.* **450** (2015), no. 1 288–294, [arXiv:1405.1566].

[148] F. Finelli, J. Garcia-Bellido, A. Kovacs, F. Paci, and I. Szapudi, *A Supervoid Imprinting the Cold Spot in the Cosmic Microwave Background*, arXiv:1405.1555.

[149] B. R. Granett, M. C. Neyrinck, and I. Szapudi, *An Imprint of Super-Structures on the Microwave Background due to the Integrated Sachs-Wolfe Effect*, *Astrophys.J.* **683** (2008) L99–L102, [arXiv:0805.3695].

[150] B. R. Granett, M. C. Neyrinck, and I. Szapudi, *A Map of the Integrated Sachs-Wolfe Signal from Luminous Red Galaxies*, *ApJ* **701** (Aug., 2009) 414–422, [arXiv:0812.1025].

[151] S. Flender, S. Hotchkiss, and S. Nadathur, *The stacked ISW signal of rare superstructures in* Λ *CDM*, *JCAP* **1302** (2013) 013, [arXiv:1212.0776].

[152] Y.-C. Cai, M. C. Neyrinck, I. Szapudi, S. Cole, and C. S. Frenk, *A Possible Cold Imprint of Voids on the Microwave Background Radiation*, *Astrophys.J.* **786** (2014) 110, [arXiv:1301.6136].

[153] S. Hotchkiss, S. Nadathur, S. Gottlöber, I. Iliev, A. Knebe, et al., *The Jubilee ISW Project – II. Observed and simulated imprints of voids and superclusters on the cosmic microwave background*, *Mon.Not.Roy.Astron.Soc.* **446** (2015) 1321–1334, [arXiv:1405.3552].

[154] B. R. Granett, A. Kovács, and A. J. Hawken, *The Integrated Sachs-Wolfe Signal from BOSS Super-Structures*, arXiv:1507.03914.

[155] J. P. Zibin and A. Moss, *Nowhere to hide: closing in on cosmological homogeneity*, arXiv:1409.3831.

[156] M. P. Mood, J. T. Firouzjaee, and R. Mansouri, *Exact general relativistic lensing versus thin lens approximation: the crucial role of the void*, arXiv:1304.5062.

[157] B. Chen, R. Kantowski, and X. Dai, *A Simple Gravitational Lens Model For Cosmic Voids*, *Astrophys.J.* **804** (2015), no. 2 130, [arXiv:1310.7574].

[158] N. Brouzakis and N. Tetradis, *Analytical Estimate of the Effect of Spherical Inhomogeneities on Luminosity Distance and Redshift*, *Phys.Lett.* **B665** (2008) 344–348, [arXiv:0802.0859].

[159] K. Gorski, E. Hivon, A. Banday, B. Wandelt, F. Hansen, M. Reinecke, and M. Bartelman, *HEALPix - A Framework for high resolution discretization, and fast analysis of data distributed on the sphere*, *Astrophys.J.* **622** (2005) 759–771, [astro-ph/0409513].

[160] M. Sasaki, *The magnitude-redshift relation in a perturbed Friedmann universe*, *MNRAS* **228** (1987) 653–669.

[161] N. Sugiura, N. Sugiyama, and M. Sasaki, *Anisotropies in Luminosity Distance*, *Progress of Theoretical Physics* **101** (1999) 903–922.

[162] C. Bonvin, R. Durrer, and M. A. Gasparini, *Fluctuations of the luminosity distance*, *Phys.Rev.* **D73** (2006) 023523, [astro-ph/0511183].

[163] R. A. Vanderveld, E. E. Flanagan, and I. Wasserman, *Systematic corrections to the measured cosmological constant as a result of local inhomogeneity*, *Phys.Rev.* **D76** (2007) 083504, [arXiv:0706.1931].

[164] I. Ben-Dayan, M. Gasperini, G. Marozzi, F. Nugier, and G. Veneziano, *Backreaction on the luminosity-redshift relation from gauge invariant light-cone averaging*, *JCAP* **4** (Apr., 2012) 36, [arXiv:1202.1247].

[165] I. Ben-Dayan, M. Gasperini, G. Marozzi, F. Nugier, and G. Veneziano, *Do Stochastic Inhomogeneities Affect Dark-Energy Precision Measurements?*, *Physical Review Letters* **110** (2013), no. 2 021301, [arXiv:1207.1286].

[166] O. Umeh, C. Clarkson, and R. Maartens, *Nonlinear relativistic corrections to cosmological distances, redshift and gravitational lensing magnification: I. Key results*, *Classical and Quantum Gravity* **31** (Oct., 2014) 202001, [arXiv:1207.2109].

[167] I. Ben-Dayan, G. Marozzi, F. Nugier, and G. Veneziano, *The second-order luminosity-redshift relation in a generic inhomogeneous cosmology*, *JCAP* **11** (2012) 45, [arXiv:1209.4326].

[168] I. Ben-Dayan, M. Gasperini, G. Marozzi, F. Nugier, and G. Veneziano, *Average and dispersion of the luminosity-redshift relation in the concordance model*, *JCAP* **1306** (2013) 002, [arXiv:1302.0740].

[169] G. Fanizza, M. Gasperini, G. Marozzi, and G. Veneziano, *An exact Jacobi map in the geodesic light-cone gauge*, *JCAP* **1311** (2013) 019, [arXiv:1308.4935].

[170] G. Marozzi, *The luminosity distance-redshift relation up to second order in the Poisson gauge with anisotropic stress*, *Classical and Quantum Gravity* **32** (Feb., 2015) 045004, [arXiv:1406.1135].

[171] O. Umeh, C. Clarkson, and R. Maartens, *Nonlinear relativistic corrections to cosmological distances, redshift and gravitational lensing magnification. II - Derivation*, *Class. Quant. Grav.* **31** (2014) 205001, [arXiv:1402.1933].

[172] G. Fanizza, M. Gasperini, G. Marozzi, and G. Veneziano, *A new approach to the propagation of light-like signals in perturbed cosmological backgrounds*, arXiv:1506.02003.

[173] C. Bonvin, C. Clarkson, R. Durrer, R. Maartens, and O. Umeh, *Cosmological ensemble and directional averages of observables*, arXiv:1504.01676.

[174] C. Bonvin, C. Clarkson, R. Durrer, R. Maartens, and O. Umeh, *Do we care about the distance to the CMB? Clarifying the impact of second-order lensing*, arXiv:1503.07831.

[175] N. Kaiser and J. A. Peacock, *On the Bias of the Distance-Redshift Relation from Gravitational Lensing*, arXiv:1503.08506.

[176] T. Kibble and R. Lieu, *Average magnification effect of clumping of matter*, *Astrophys.J.* **632** (2005) 718–726, [astro-ph/0412275].

[177] M. Troxel, M. Ishak, and A. Peel, *The effects of structure anisotropy on lensing observables in an exact general relativistic setting for precision cosmology*, *JCAP* **1403** (2014) 040, [arXiv:1311.5936].

[178] F. K. Hansen, A. Banday, and K. Gorski, *Testing the cosmological principle of isotropy: Local power spectrum estimates of the WMAP data*, *Mon.Not.Roy.Astron.Soc.* **354** (2004) 641–665, [astro-ph/0404206].

[179] F. Hansen, A. Banday, K. Gorski, H. Eriksen, and P. Lilje, *Power Asymmetry in Cosmic Microwave Background Fluctuations from Full Sky to Sub-degree Scales: Is the Universe Isotropic?*, *Astrophys.J.* **704** (2009) 1448–1458, [arXiv:0812.3795].

[180] M. Vonlanthen, S. Rasanen, and R. Durrer, *Model-independent cosmological constraints from the CMB*, *JCAP* **1008** (2010) 023, [arXiv:1003.0810].

[181] B. Audren, J. Lesgourgues, K. Benabed, and S. Prunet, *Conservative constraints on early cosmology with MONTE PYTHON*, *JCAP* **2** (2013) 1, [arXiv:1210.7183].

[182] B. Audren, *Separate Constraints on Early and Late Cosmology*, *Mon.Not.Roy.Astron.Soc.* **444** (2014), no. 1 827–832, [arXiv:1312.5696].

[183] K. Rosquist, *Trigonometric parallaxes of distant objects - What they could tell about the universe*, *ApJ* **331** (1988) 648–652.

[184] V. Perlick, *Gravitational Lensing from a Spacetime Perspective*, *Submitted to: Living Rev. Rel.* (2010) [arXiv:1010.3416].